(12) INTERNATIONAL APPLICATION PUBLISHED UNDER THE PATENT COOPERATION TREATY (PCT)

(19) World Intellectual Property Organization
International Bureau

(43) International Publication Date
24 November 2016 (24.11.2016)

WIPO | PCT

(10) International Publication Number
WO 2016/184329 A1

(51) International Patent Classification:
G02B 6/12 (2006.01)

(21) International Application Number:
PCT/CN2016/081533

(22) International Filing Date:
10 May 2016 (10.05.2016)

(25) Filing Language: English

(26) Publication Language: English

(30) Priority Data:
62/162,000 15 May 2015 (15.05.2015) US
15/013,538 2 February 2016 (02.02.2016) US

(71) Applicant: **HUAWEI TECHNOLOGIES CO., LTD.** [CN/CN]; Huawei Administration Building, Bantian, Longgang District, Shenzhen, Guangdong 518129 (CN).

(72) Inventors: **LU, Zeqin**; Unit 2143, 6335 Thunderbird Crescent, Vancouver, British Columbia V6T 2G9 (CA). **MURRAY, Kyle Jacob**; 2205 Lower Mall, Vancouver, British Columbia V6T 1Z4 (CA). **CHROSTOWSKI, Lukas**; 504-6333 Larkin Drive, Vancouver, British Columbia V6T 0A7 (CA).

(81) Designated States *(unless otherwise indicated, for every kind of national protection available)*: AE, AG, AL, AM, AO, AT, AU, AZ, BA, BB, BG, BH, BN, BR, BW, BY, BZ, CA, CH, CL, CN, CO, CR, CU, CZ, DE, DK, DM, DO, DZ, EC, EE, EG, ES, FI, GB, GD, GE, GH, GM, GT, HN, HR, HU, ID, IL, IN, IR, IS, JP, KE, KG, KN, KP, KR, KZ, LA, LC, LK, LR, LS, LU, LY, MA, MD, ME, MG, MK, MN, MW, MX, MY, MZ, NA, NG, NI, NO, NZ, OM, PA, PE, PG, PH, PL, PT, QA, RO, RS, RU, RW, SA, SC, SD, SE, SG, SK, SL, SM, ST, SV, SY, TH, TJ, TM, TN, TR, TT, TZ, UA, UG, US, UZ, VC, VN, ZA, ZM, ZW.

(84) Designated States *(unless otherwise indicated, for every kind of regional protection available)*: ARIPO (BW, GH, GM, KE, LR, LS, MW, MZ, NA, RW, SD, SL, ST, SZ, TZ, UG, ZM, ZW), Eurasian (AM, AZ, BY, KG, KZ, RU, TJ, TM), European (AL, AT, BE, BG, CH, CY, CZ, DE, DK, EE, ES, FI, FR, GB, GR, HR, HU, IE, IS, IT, LT, LU, LV, MC, MK, MT, NL, NO, PL, PT, RO, RS, SE, SI, SK, SM, TR), OAPI (BF, BJ, CF, CG, CI, CM, GA, GN, GQ, GW, KM, ML, MR, NE, SN, TD, TG).

Declarations under Rule 4.17:

— *as to the applicant's entitlement to claim the priority of the earlier application (Rule 4.17(iii))*

Published:

— *with international search report (Art. 21(3))*

(54) **Title**: OPTICAL PHASE SHIFTER

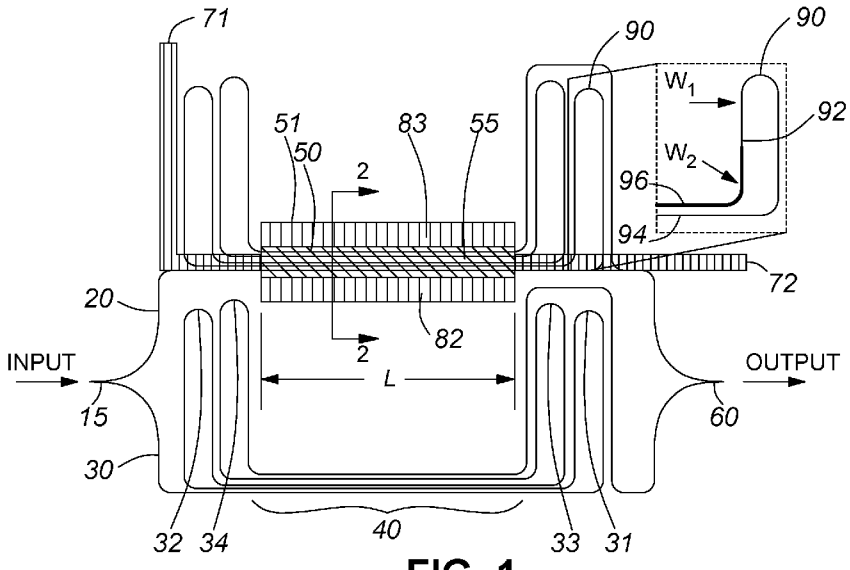

FIG. 1

(57) **Abstract**: An optical device comprises first and second waveguide phase arms (20, 30) and a tunable element. Each of first and second waveguide phase arms (20, 30) has optically coupled parallel sections of waveguides. The parallel sections of each one of the first and second waveguide phase arms (20, 30) being dissimilar to lessen crosstalk. The tunable element applies a phase shift to an optical signal traversing the first waveguide phase arm.

WO 2016/184329 A1

OPTICAL PHASE SHIFTER

CROSS REFERENCE TO RELATED APPLICATIONS

[0001] This application claims the benefit of priority to US Patent Application No. 15/013,538 entitled "Optical Phase Shifter" filed Feb 02, 2016, which claims the benefit of priority to US Patent Application Serial Number 62/162,000 entitled "Optical Phase Shifter" filed May 15, 2015, both of which are hereby incorporated by reference in its entirety.

FIELD OF THE DISCLOSURE

[0002] The present disclosure relates to optical components.

BACKGROUND

[0003] Optical switches that are low-cost, low-power, and of a compact size are important components in optical cross connects (OXC) and reconfigurable optical add-drop multiplexers (ROADM). Silicon-on-insulator (SOI) is a promising technology for developing optical switches due to its relatively large thermo-optic coefficient, high thermal conductivity and high contrast refractive index. In recent years, various thermo-optic switch configurations have been reported on the SOI platforms.

[0004] Phase shifters are used in many silicon photonic devices, including switches, modulators and tunable filters. Two common ways of implementing a phase shifter rely on an electro-optic effect, in which a change in the density of charge carriers affects the refractive index of silicon, and a thermo-optic effect, in which a temperature change affects the refractive index. Electro-optic phase shifters, while having fast operation, may require large footprints or high operating voltages and have an optical loss modulation associated with the phase shift. Thermo-optic phase shifters can achieve large phase shifts in small footprints with low operating voltages and without introducing optical loss modulation. However, they have slower response times and typically require more power for switching.

[0005] Much work has been devoted to reducing the power consumption of thermo-optic switches. Similarly, there is a need to improve the efficiency of optical phase shifters which are used in thermo-optic switches.

SUMMARY

[0006] An aspect of the disclosure provides an optical device which uses thermo-optic properties of Silicon-On-Insulator, along with a tunable element, to provide an optical phase shifter with an improved power consumption profile. Accordingly, an optical device is disclosed which includes first and second waveguide phase arms each having an optically coupled parallel section of waveguides, the parallel sections of the waveguide phase arms being dissimilar to prevent crosstalk. The device further includes a tunable element for applying a phase shift to an optical signal traversing the first phase arm. In some embodiments, each optically coupled parallel section of waveguides forms a single lightpath. In some embodiments the waveguides of the parallel sections have dissimilar dimensions, which can vary in width, thickness and/or gap. In some embodiments the devices are fabricated to include parallel sections of dissimilar waveguides coupled together to form a single lightpath.

[0007] In accordance with embodiments of the present disclosure, there is provided an optical device comprising a coupler, first and second waveguides and a tunable element. The coupler is configured as an input power splitter and an output power combiner. The first and second waveguide phase arms are each folded in a plurality of turns to form arms with aligned sections. Optionally, there are two waveguide reflectors at the end of the phase arms. The tunable element is associated with the first phase arm. An embodiment is directed to a Michelson interferometer configuration with a suspended phase arm and densely folded waveguides of different widths to prevent crosstalk and for thermal efficiency.

[0008] Embodiments include a thermo-optic switch based on a Michelson interferometer configuration comprising a 2x2 adiabatic coupler which works as the input power splitter and output power combiner, two waveguide phase arms that are folded by a plurality of turns, and two waveguide loop mirrors working as reflectors at the end of the phase arms. The loop mirrors can be formed with a compact Y-branch and bent waveguides. One of the phase arms, designed for thermal tuning, is thermally isolated from the other arm with thermal undercut

trenches. Some of the underlying Si substrate between the trenches is removed to form a suspended arm. A heating element is placed on top of the suspended arm for thermal tuning. Waveguide interaction length with the heater is increased by folding the waveguide multiple times. To increase the number of waveguides underneath the heater, the number of folded waveguides within the suspended region is maximized by designing waveguides with dissimilar widths.

[0009] In accordance with an aspect of the disclosure, there is provided an optical device including first and second waveguide phase arms each having optically coupled parallel sections of waveguides, the parallel sections of each one of the first and second waveguide phase arms being dissimilar to lessen crosstalk. The optical device further includes a tunable element for applying a phase shift to an optical signal traversing the first waveguide phase arm. In some embodiments, each optically coupled parallel section of waveguides forms a single lightpath. In some embodiments, waveguides of the parallel sections have dissimilar dimensions. In some embodiments, waveguides of the parallel sections have dissimilar dimensions which vary in one or more of gap, width, and/or thickness. In some embodiments, adjacent waveguides of the parallel sections have dissimilar dimensions. In some embodiments, the first and second waveguide phase arms comprise a plurality of tapered waveguides of different dimensions which are connected by loops, and the loops form transitions between the different dimensions. In some embodiments, there are N parallel sections and N-1 loops, with N being an odd integer greater than or equal to 3, such that input and output signals in each one of the first and second waveguide phase arms travel in a same direction. In some embodiments, the tunable element comprises a thermo-optic heater thermally coupled to the first waveguide phase arm. In some embodiments, the optical device is a silicon photonic device, wherein the thermo-optic heater comprises a metallic layer. In some embodiments, the first waveguide phase arm is suspended for better thermal isolation thereof. In some embodiments, the optical device in the region of the thermo-optic heater is underetched to improve thermal isolation of the first waveguide phase arm adjacent the thermo-optic heater. In some embodiments, the optical device further includes a coupler configured as both an input power splitter for splitting an input optical signal between the first and second waveguide phase arms, and as an output power combiner for recombining optical signals from the first and second waveguide phase arms to produce an output optical signal. In some embodiments, the

optical device is configured as a Michelson interferometer, and wherein the first and second waveguide phase arms are terminated with waveguide reflectors at ends of the first and second waveguide phase arms. In some embodiments, the one or more couplers comprise a 2x2 coupler selected from a group consisting of an adiabatic coupler, a multimode interference (MMI) coupler, and a directional coupler. In some embodiments, the waveguide reflectors comprise loop mirrors. In some embodiments, the loop mirror comprises a compact Y-branch and a bent waveguide. In some embodiments, the optical device is configured as a thermo-optic switch. In some embodiments, the optical device further includes one or more couplers configured as input power splitters for splitting an input optical signal between the first and second waveguide phase arms, or as output power combiners for recombining the optical signal from the first and second waveguide phase arms to produce an output optical signal. In some embodiments the optical device is configured as a tunable Mach-Zehnder interferometer based optical switch. In some embodiments, the optical device is configured as a modulator. In some embodiments, the optical device is configured as a tunable Mach-Zehnder interferometer wherein at least adjacent waveguides of the parallel sections have varying widths.

BRIEF DESCRIPTION OF THE FIGURES

[0010] Further features and advantages of the present disclosure will become apparent from the following detailed description, taken in combination with the appended drawings, in which:

[0011] Figure 1 shows a schematic diagram of a phase shifter device according to an embodiment.

[0012] Figure 2 is cross-section of the phase shifter region along line 2-2 of Figure 1 for an underetched device.

[0013] Figure 3 is similar to Figure 2, but for a device without underetching.

[0014] Figure 4 is a schematic diagram of a parallel waveguide structure according to an embodiment.

[0015] Figure 5 is a schematic top view of another embodiment of a thermo-optic switch.

[0016] Figure 6 is a cross-section of the suspended region along line 6-6 of Figure 5;

[0017] Figure 7 shows an enlargement of the inset from Figure 5 illustrating an example region for the transition of dissimilar waveguides.

[0018] Figure 8 illustrates a dissimilar waveguide structure and horizontal electric field profile of its modes according to an embodiment.

[0019] Figure 9 illustrates maximum crosstalk between 220 nm thick waveguides with 1 mm pitch.

[0020] Figure 10A shows the calculated spectra of the folded waveguide structure, and Figure 10B shows the results according to an embodiment.

[0021] Figures 11A and 11B show example optical spectra of the underetched versions of embodiments of MZI devices 3 and 5, respectively, in the on and off state.

[0022] Figures 12A-D show the normalized transmission functions of the unetched and underetched versions of embodiments of MZI devices 2-5 as functions of the power applied to the thermal phase shifter, along with sinusoidal fits to the data.

[0023] Figures 13A-B show temporal responses of a) unetched, and b) underetched MZI switches respectively according to embodiments.

[0024] Figure 14 shows the maximum coupling at 1550 nm between two dissimilar waveguides with widths of 400 nm, 500 nm, and 600 nm according to example Michelson Interferometer Configuration (MIC) devices.

[0025] Figures 15A-C show measurement results for MIC device 6. Figure 15A shows optical transmission at switching ON and OFF states; Figure 15B shows transmission at 1550 nm as a function of tuning power and Figure 15C shows time-domain responses at 1550 nm.

[0026] Figures 16A and B show a performance comparison of the embodiment test devices. Figure 16A shows switching power and Figure 16B shows response time. In both, the dash lines are fitting curves for measurement results.

[0027] Figure 17 is a 3D heat transfer simulation for the suspended arm of MIC device 6 according to an embodiment. The arrows indicate the heat flux. The size of the arrows indicates the magnitude of the heat flux.

[0028] It will be noted that throughout the appended drawings, like features are identified by like reference numerals.

DETAILED DESCRIPTION

[0029] While power budget has been continuously reduced, published works have not been able to demonstrate power levels that satisfy high density photonic network requirements. Solving power budget issues will create new opportunities for large switch matrix application.

[0030] A number of methods for increasing the efficiency of thermal phase shifters have been proposed. These methods include improving thermal isolation by removing the material surrounding the phase shifters and folding a waveguide many times under a heater to increase the optical interaction length within the heated region. It is pointed out that semiconductor waveguides are fabricated, but the term folding is used to describe the shape that would be achieved by folding a single fiber.

[0031] When folding a waveguide under a heater, the waveguide spacing between each fold is limited by the evanescent coupling of light between adjacent waveguides. When adjacent waveguides are identical to each other, the coupling of power between them is resonant, and a complete transfer of power can be achieved over a characteristic coupling length. The coupling length is strongly dependent on the waveguide spacing, and so the spacing must be chosen such that the power coupling over the length of the device is sufficiently small for the desired application. This need for a sufficiently large spacing limits the achievable density of waveguide routing and therefore limits the number of times a waveguide can be folded under a heater and thus subsequently limits the power efficiency gains which can be achieved. In other

words, crosstalk occurs when parallel waveguides are close to each other. This crosstalk can be reduced by sufficiently spacing apart the parallel waveguides. However, devices with sufficient separation of the waveguides to reduce crosstalk to acceptable levels have an increased size both in terms of footprint and heater size.

[0032] Presented below is a configuration in which different waveguide dimensions in the parallel sections (e.g. folds) of the phase shifter are used to overcome the limits imposed by the requirement for sufficiently large spacing discussed above. The evanescent coupling between dissimilar waveguides does not achieve phase matching. Therefore, the power coupling between dissimilar waveguides is not complete. For a given waveguide spacing, if the mismatch between adjacent waveguide widths is sufficiently large, then the power coupling can be made negligibly small over any coupling length. Without the need to have a large spacing, the density of waveguide folding under a heating element can be increased dramatically, and the efficiency of thermal heaters can be correspondingly improved.

[0033] Improved phase shifters which can either be used as modulators or form thermo-optic switches are disclosed. Some embodiments utilize a Mach-Zehnder interferometer (MZI) configuration, whereas other embodiments utilize Michelson interferometer configurations. Each use first and second waveguide phase arms. Each phase arm has a plurality of optically coupled parallel sections, which can be described as zigzag folded waveguides. Each device also includes a tunable element (for example a heater) for applying a phase shift to an optical signal traversing the first phase arm. The folded waveguides are used to increase the waveguide interaction length with the heated region. The parallel sections of the waveguide phase arms are configured to be dissimilar to prevent crosstalk. In some embodiments, thermal isolation of the tuning regions is used to further reduce switching power. In some embodiments, suspended structures are used to achieve better thermal isolation. While MZI and Michelson interferometer configurations are discussed, it should be appreciated that other configurations can be used.

[0034] Additionally, dissimilar waveguides can increase waveguide routing density in photonic circuits. Dissimilar waveguide routing may also be used for dense mode division multiplexing with gaps between adjacent waveguides as small as 100 nm.

[0035] Embodiments will be discussed in which the thickness is the same for all waveguides and the width varies. However, other embodiments could use different thicknesses and the same width, or have both different (in fact it is believed that varying both would allow for designs with the best performance). Other embodiments can vary the gap between waveguide sections.

[0036] Figure 1 shows a schematic diagram of an optical device implemented using an MZI configuration, according to an embodiment. Input light is split by a coupler, for example a 50-50 adiabatic splitter **15,** into a first phase arm **20** and a second phase arm **30**. The two phase arms are similar in configuration, except the first (upper) phase arm **20** passes through a heater **55**. Each phase arm includes a dense dissimilar waveguide routing region **40**, which in this illustration is the parallel section **40** of 5 sections of waveguides of length L. Each waveguide is folded 4 times. As mentioned above, some embodiments are directed to fabricated semiconductor waveguides, which would be fabricated and not actually folded. Looking at light traversing the second (lower) phase arm **30**, it can be seen that the light would pass through first parallel section at **40** before looping back via a first fold **31** to loop back at a second fold **32** to traverse the parallel section **40** again before looping back at fold **33** and then fold **34** before recombining with the light from the first phase arm at coupler **60** at the output of the device.

[0037] Accordingly, it can be seen that there is a single lightpath for each phase arm, with each phase arm including parallel sections of waveguides (5 are illustrated, but this number can vary). In general, the light travelling along the upper MZI arm **20** passes N times through a thermal phase shifter **51** before recombining with the light from the other arm at the device output, wherein N=5 in the embodiment shown.

[0038] The thermal phase shifter **51** comprises a suspended structure **50**, which may be formed from SiO_2, and the heater **55** of length L which heats the parallel section of waveguides **40** of the first phase arm **20**. The heater **55** is connected to routing metal strips **71, 72** which provide the input current to control the heater **55**. In this embodiment, the parallel section **40** of the waveguides and the heater **55** forms the suspended structure **50**, which is thermally separated from the surrounding portions of optical device. In this embodiment, the suspended structure **50** is formed by etching the surrounding portions of the SiO2 to form trenches **82, 83**,

and in the case of an underetched device, the area underneath **85**, which can be seen more clearly in Figure 2.

[0039] It is useful to increase the number of waveguides within the parallel section in order to increase the length of optical interaction with the heater. Prior art devices have accomplished this by folding a single waveguide multiple times to form a parallel section under the heater. However, as discussed above, parallel waveguides can cause crosstalk. To prevent parallel waveguides from causing crosstalk, waveguides with different dimensions are utilized in the parallel sections. While it is known that crosstalk can be reduced between parallel waveguides of different lightpaths by utilizing different waveguide widths, embodiments of the present invention now extend this principle for parallel waveguide sections of a single lightpath.

[0040] As shown in the inset of Figure 1 (and as can be seen in Figure 2), the widths of the waveguides of the parallel sections are designed to be dissimilar with widths w_1, w_2,..., w_N, in order to obtain dense routing while keeping crosstalk between the waveguides sufficiently small. The evanescent coupling between the dissimilar waveguides does not achieve the phase matching condition so that power transfer between the waveguides is negligible.

[0041] It is noted that the term "parallel section" is used for ease of explanation. For optimal performance with minimum footprint, it is desirable (but not necessary) for the waveguides to be substantially parallel. If the waveguides are not parallel, then they will be diverging (in the region of the heater), thus increasing the footprint and reducing thermal efficiency, or converging and increasing crosstalk. Both are undesirable, but many applications can trade-off some degree of either in order to reduce the cost of optimally aligning the waveguides. Accordingly, it is to be understood that, in some embodiments, the parallel sections of waveguides can allow some divergence from parallel, and the term "parallel section" shall be construed to allow for such a divergence.

[0042] In one embodiment, tapered waveguides are used for a transition **92** between the dissimilar waveguide portions of the phase arms, as shown in the insert of Figure 1. As illustrated, a first waveguide **94** having width $\mathbf{W_1}$ is inserted into a second waveguide **96** having width $\mathbf{W_2}$ at the transition **92** in a loop **90**. The tapered waveguides are shown to transition at the loops in order that the aligned portions not cause crosstalk. The transition need not necessarily be part of the loop. However, other mechanisms for coupling dissimilar

waveguides can be used. For example, in another embodiment, a series of N waveguides of different widths are joined by conventional loops. This may result in transitions that occur when the waveguides are still parallel. This may introduce a small amount of crosstalk in the portions where the waveguides have the same widths and are parallel. However, such a small amount of crosstalk may be acceptable for some applications.

[0043] Figure 2 is a cross-section of the phase shifter region along line 2-2. In Figure 2, the heater **55** has a width of 10 μm. The heater **55** is used to apply a temperature change to the waveguides to induce a thermo-optic phase shift. In some embodiments, the heater **55** is a metallic heater. In some embodiments, the optical device is a silicon photonic device comprising SiO_2 housing for silicon waveguides. In some embodiments, the heater **55** is formed from a deposited metallic layer, for example TiN. The dimensions of the waveguides are as follows. Each of the N waveguides has a thickness **T** of 220 nm, a width, $\mathbf{W_i}$, i=1,2…N, and all waveguides are separated by a common gap **g**. The device includes passages or trenches **82, 83**, which can be oxide openings or etched to provide thermal isolation. In some embodiments, the silicon substrate (which may be formed from SiO_2) has been removed (e.g., by underetching area **85**) to form the suspended bridge structure **50** having a width of 12 μm to increase thermal isolation. To avoid crosstalk, the parallel sections of the waveguide phase arms have dissimilar dimensions. In the embodiments discussed, the waveguides have the same thickness and are made dissimilar by varying the width. However, dissimilar waveguides which can vary in one or more of gap, width, and/or thickness can be used.

[0044] Figure 3 is similar to Figure 2, but illustrates a similar cross section for a device without underetching. Figure 3 can be thought of as a view of the device of Figure 2 before underetching of the area **85**, showing the unetched silicon substrate **86** underneath the waveguides. As the device in Figure 3 is not underetched, the reference numeral **50** is removed as it is not a suspended structure, but it still has some measure of thermal isolation from the rest of the device via trenches **82, 83**.

[0045] It should be noted that embodiments can be configured with a number of variations for providing thermal isolation of the waveguides in the vicinity of the heater, including:

i) no etching of trenches or underetching;

ii) isolation trenches (**82,83**) formed by removal of the oxide and/or substrate horizontally adjacent to the waveguides; and/or

iii) removal of the substrate **86** underneath the waveguides to under-etch the area **85**

[0046] The optical device shown in Figure 1 could be implemented as a modulator, attenuator, switch, etc.

[0047] Figure 4 shows a schematic of the parallel section of length L for N waveguides forming a single lightpath. As can be seen, the dimensions of each waveguide in the parallel section varies with widths $\mathbf{W_m}$, for m = 1,2…*N*. Light is injected into the waveguide at the input and propagates through each waveguide through loops (not shown), such that the transmitted light can be measured at the output from waveguide *N*. An odd number of waveguides is considered so that the input and transmitted light are travelling in the same direction **Z**.

[0048] Another embodiment provides a phase shifter which can be used in an optical switch that incorporates a Michelson interferometer configuration, suspended structures, and parallel waveguides to further reduce the power consumption of SOI thermo-optic switches.

[0049] A top schematic view of a Michelson interferometer thermo-optic switch according to an embodiment is shown in Figure 5. The embodiment includes a 2x2 adiabatic coupler **510**, which functions as an input power splitter and output power re-combiner. However, other couplers could be used, including MMI, directional couplers, etc. The input light is split between two waveguide phase arms, namely first phase arm **520** and second phase arm **530**. Both phase arms include a plurality of folds or loops **522, 523, 534, 535** to produce optically coupled parallel sections of waveguide **540**, and two waveguide loop mirrors **521, 531** functioning as reflectors at the end of the phase arms. An example look **533** will be discussed below with reference to Figure 7. In an embodiment, the loop mirrors **521, 531** are formed using a compact Y-branch and bent waveguides. However, other types of loop mirrors can be used, including those formed from an adiabatic or other splitter instead of a Y-branch.

[0050] The first phase arm includes a series of 5 suspended structures **600**, each being 45 μm long and separated by 6 μm, through which a heater **610** is disposed.

[0051] Figure 6 is a cross-section through one of the suspended structures **600** along line 6-6 of Figure 5. The heater **610** having e.g. a width of 8 μm and length L is used to apply a temperature change to the waveguides to induce a thermo-optic phase shift. In some embodiments, the heater **610** is a metallic heater. In some embodiments, the optical device is a silicon photonic device comprising SiO_2 housing for silicon waveguides. In some embodiments, the heater **610** is formed from a deposited metallic layer, for example TiN. The dimensions of the waveguides are as follows. Each of the N waveguides has a thickness **T** of 220 nm, a width $\mathbf{W_i}$, i=1,2…N, and all waveguides are separated by a common gap **g**. The device includes passages or trenches **620, 630**, which can be oxide openings or etched to provide thermal isolation. In some embodiments, the silicon substrate (which may be formed from SiO_2) is removed (e.g., by underetching the area **640)** to form a 12 μm wide suspended bridge **650** to increase the thermal isolation.

[0052] Accordingly there are a number of possibilities, including:

i) The parallel waveguide section is thermally isolated at both sides (**620, 630**) and underneath **640**, as illustrated in Figure 6, which will be referred to as a suspended structure in Figures 16A and 16B ;

ii) The parallel waveguide section is thermally isolated at the sides **620**, **630** but not underneath **640**; and

iii) The parallel waveguide section is not thermally isolated at the sides or underneath (which will be referred to as without suspended structures in Figures 16A and 16B).

[0053] To reduce crosstalk, the parallel sections of the waveguide phase arms may have dissimilar dimensions. In the embodiments discussed, the waveguides have the same thickness and are made dissimilar by varying the width. However, dissimilar waveguides which can vary in width, thickness or both can be used. Further, the gap between the waveguides can also be varied.

[0054] Figure 7 illustrates the inset from Figure 5. Figure 7 illustrates an example loop **533** and the transition between dissimilar waveguides, wherein the lightpath transitions from a waveguide of width W_{N-1} to a width of W_N, using for example tapered waveguides. The radii of the waveguide bends are 5 μm. The tapered waveguides are shown to transition at the loops in order that the aligned portions not cause crosstalk however, as stated above, other mechanisms for coupling dissimilar waveguides can be used.

[0055] Cross coupling in Mach Zehnder interferometers utilizing folded waveguides is modeled to show that the ripple in the through spectrum of the switch is an appropriate metric for measuring the degree of crosstalk present.

[0056] A theoretical model involving Coupled Mode Theory of Dissimilar Waveguides will now be discussed. In this section, the crosstalk between a pair of dissimilar waveguides is computed. To achieve this, a notion of the power in a waveguide is defined by projecting the optical field of the two waveguide system onto the field of a single waveguide mode. A change of basis from the two-waveguide eigenmode basis is discussed, in which the propagation is simple to describe, to a basis in which the power in each waveguide is simple to compute. In this basis, the propagation is more complicated due to the appearance of coupling between modes.

[0057] Figure 8 illustrates dissimilar waveguide structure and horizontal electric field profile of its modes. Modes $|1\rangle$ and $|2\rangle$ are the modes of the two-waveguide structure. Modes $|A_0\rangle$ and $|B_0\rangle$ are the modes when only waveguide A or waveguide B are present respectively.

[0058] Consider two parallel waveguides, denoted as waveguides A and B, of thickness t and widths W_A and W_B separated by a gap, g, as shown in Figure 8. The two waveguide system has transverse electric (TE) eigenmodes $|1\rangle$ and $|2\rangle$, each normalized to unit power, with propagation constants k_1 and k_2 respectively. Waveguides A and B considered in isolation have eigenmodes $|A_0\rangle$ and $|B_0\rangle$, respectively, the inner product:

$$\langle \psi_1 | \psi_2 \rangle = \frac{1}{4}\left[\iint E_1 \times H_2^* \cdot dS + \int E_2^* \times H_1 \cdot dS\right] \quad (1)$$

where E_i and H_i, i = 1,2 are transverse electric and magnetic field profiles of two modes $|\psi_1\rangle$ and S is the plane normal to the propagation direction, we can decompose the single waveguide state $|A_0\rangle$ in terms of the two-waveguide eigenmodes:

$$|A\rangle = \langle 1|A_0\rangle |1\rangle + \langle 2|A_0\rangle |2\rangle . \tag{2}$$

[0059] The difference between $|A\rangle$ and $|A_0\rangle$ is due to not including the complete set of radiation modes in the mode decomposition. Define the power normalized state

$$|\bar{A}\rangle = \frac{|A\rangle}{\sqrt{\langle A|A\rangle}}, \tag{3}$$

and $|\bar{B}\rangle$ similarly. A general superposition in the $|1\rangle$ and $|2\rangle$ basis is then denoted as a vector with the components *a* and *b*:

$$\mathbf{V} = \begin{bmatrix} a \\ b \end{bmatrix} = a|1\rangle + b|2\rangle . \tag{4}$$

[0060] Evolution along the propagation direction, *z* provides:

$$\frac{d\mathbf{V}}{dz} = i\begin{bmatrix} k_1 & 0 \\ 0 & k_2 \end{bmatrix}\mathbf{V} \equiv i\mathbf{P}\mathbf{V}. \tag{5}$$

[0061] Performing a change to the $|\bar{A}\rangle, |\bar{B}\rangle$ basis with components *c* and *d*,

$$\bar{\mathbf{V}} = \begin{bmatrix} c \\ d \end{bmatrix} = c|\bar{A}\rangle + d|\bar{B}\rangle \tag{6}$$

$$\mathbf{V} = \begin{bmatrix} \frac{\langle 1|A_0\rangle}{\sqrt{\langle A|A\rangle}} & \frac{\langle 1|B_0\rangle}{\sqrt{\langle B|B\rangle}} \\ \frac{\langle 2|A_0\rangle}{\sqrt{\langle A|A\rangle}} & \frac{\langle 2|B_0\rangle}{\sqrt{\langle B|B\rangle}} \end{bmatrix} \tilde{\mathbf{V}} \equiv M\tilde{\mathbf{V}}, \tag{7}$$

[0062] The new evolution follows:

$$\frac{d\tilde{\mathbf{V}}}{dz} = iM^{-1}PM\tilde{\mathbf{V}} \equiv i\tilde{P}\tilde{\mathbf{V}}. \tag{8}$$

[0063] It should be noted that since in general M is not unitary the inner product is

$$\mathbf{V}^{\dagger}\mathbf{V} = \tilde{\mathbf{V}}^{\dagger}M^{\dagger}M\tilde{\mathbf{V}} \neq \tilde{\mathbf{V}}^{\dagger}\tilde{\mathbf{V}} \tag{9}$$

and the sum of the squares of the norms of the components of $\overline{V}$ is not in general a conserved quantity. Nevertheless, we will identify the square of the norms of the components of $\overline{V}$ with the informal notation of the power contained in each waveguide. More precisely, the square of the norm of the first component of $\overline{V}$ is the power that would be transmitted into waveguide A if waveguide B were abruptly terminated and the squared norm of the second component has a similar interpretation.

[0064] Considering a situation where at z = 0 the waveguide system is excited in the state $\left|\overline{A}\right\rangle$, then one can consider the power coupled to waveguide B over some length L as the squared norm of the amplitude of $\left|\overline{B}\right\rangle$ at z = L. In the special case where waveguides A and B are identical, the power is transferred completely from waveguide A to waveguide B over a characteristic length, $L_c = \pi/(k_1-k_2)$, depending on the dimensions of the waveguides and their separation [11]. Thus to limit the crosstalk between the waveguides over their length then the separation between the waveguides should be made large enough such that $L_c >> L$.

[0065] If the two waveguides are not identical, then the power is still periodically coupled between the waveguides, but the transfer of power is incomplete. The maximum crosstalk, CT,

can then be computed as the maximum value of the squared norm of the second component of $\bar{V}$ in the solution to Eq (8):

$$\bar{\mathbf{V}}(z) = M^{-1} e^{iP_z} M\, \bar{\mathbf{V}}(0) = M^{-1} e^{iP_z} M \begin{bmatrix} 1 \\ 0 \end{bmatrix} \tag{10}$$

$$\mathrm{CT} = \max_z \left(\left| [0\ \ 1]\, \bar{\mathbf{V}}(z) \right|^2 \right) = \max_z \left(\left| [0\ \ 1] M^{-1} e^{iP_z} M \begin{bmatrix} 1 \\ 0 \end{bmatrix} \right|^2 \right) \tag{11}$$

$$= 4 \cdot \frac{\langle B|B\rangle}{\langle A|A\rangle} \cdot \frac{|\langle 1|A_0\rangle \langle 2|A_0\rangle|^2}{|\langle 1|A_0\rangle \langle 2|B_0\rangle - \langle 1|B_0\rangle \langle 2|A_0\rangle|^2}$$

[0066] Figure 9 shows the computed maximum crosstalk for waveguides with a fixed center to center separation of 1 μm and thickness 220 nm as the widths of the waveguides are varied for a wavelength of 1550 nm. The modes and propagation constants were computed using a numerical mode solver. It can be seen that by making the waveguide widths sufficiently different the crosstalk can be limited for small separations regardless of the length of the coupler. The asymmetry of the crosstalk under interchange of waveguides A and B is due the difference between first exciting state |A⟩, then later measuring state |B⟩, and first exciting state |B⟩ then later measuring state |A⟩. This difference is due to the non-orthogonality of |A⟩ and |B⟩ for dissimilar waveguides.

[0067] Referring back to Figure 4, to model the propagation, a tight-binding coupled mode model is utilized where only the coupling between nearest neighbor waveguides is considered. The propagation is described by the differential equations:

$$\frac{d\bar{\mathbf{V}}_m^+}{dz} = a_m \bar{\mathbf{V}}_m^+ + b_m \bar{\mathbf{V}}_{m-1}^+ + c_m \bar{\mathbf{V}}_{m+1}^+ \tag{12}$$

$$\frac{d\bar{\mathbf{V}}_m^-}{dz} = -a_m \bar{\mathbf{V}}_m^- - b_m \bar{\mathbf{V}}_{m-1}^- - c_m \bar{\mathbf{V}}_{m+1}^-, \tag{13}$$

where

$\bar{V}_m^+$ and $\bar{V}_m^-$, $m = 1, 2, \ldots N$,

are the amplitudes of the modes in waveguide j travelling in the positive and negative z directions. Here a_m, b_m, and c_m are the pairwise self and cross coupling coefficients computed as described in Eq. (8). Specifically, a_m are the self-coupling coefficients found as the diagonal elements of $i\overline{P}$, and b_m and c_m are the cross-coupling coefficients found as the off-diagonal elements of $i\overline{P}$. Further, the system adheres to the boundary conditions:

$$\bar{V}_0^+(0) = 1 \tag{14}$$

$$\bar{V}_N^-(L) = 0 \tag{15}$$

$$\left.\begin{aligned} \bar{V}_m^-(L) &= \bar{V}_{m-1}^+(L)e^{i\Phi_{m-1}} \\ \bar{V}_m^+(L) &= \bar{V}_{m-1}^-(L)e^{-i\Phi_{m-1}} \end{aligned}\right\} \text{for } m \text{ even} \tag{16}$$

$$\left.\begin{aligned} \bar{V}_m^-(0) &= \bar{V}_{m-1}^+(0)e^{i\Phi_{m-1}} \\ \bar{V}_m^+(0) &= \bar{V}_{m-1}^-(0)e^{-i\Phi_{m-1}} \end{aligned}\right\} \text{for } m \text{ odd}, m > 1, \tag{17}$$

where Φ_m is the phase associated with the bend connecting waveguide m with waveguide m+1. The system of Equations (12, 13), obeying the boundary conditions given by Equations (14-17) was numerically solved for N = 9, L = 90 μm, and identical waveguides of thickness 220 nm and width 500 nm for gaps g = 500 nm, 750 nm, and 1 μm, as well as for a system consisting of alternating waveguides of widths 500 nm and 600 nm with a gap of 500 nm. The phases Φ_j were all set to zero for simplicity. The results as a function of wavelength are presented in Figure 10A, which shows the calculated spectra of the folded waveguide structure for 9 identical waveguides with gaps g_I = 500 nm, 750 nm, and 1000 nm, and alternating dissimilar waveguides with widths of 500 nm and 600 nm with gap g_D = 500 nm,

[0068] In the case of identical waveguides, there is already significant ripple in the spectrum for a gap of 750 nm and a stop band appears for a gap of 500 nm. With the dissimilar waveguides, however, the ripple in the spectrum for a gap of 500 nm is less than that for the identical waveguides at a gap of 1 μm. The shape of the spectrum depends strongly on the phases Φj, however the degree of ripple in the spectrum does not. The degree of ripple can be characterized by computing the minimum transmission of the folded waveguide structure as the gap between the waveguides was varied. The results of such a simulation are presented in

Figure 10B, which shows the minimum transmission of the folded waveguide structure. It can be seen that for the identical waveguides, the ripple in the spectrum causes the transmission to rapidly fall off for waveguide separations less than approximately 700 nm. On the other hand, the reduction in crosstalk between the dissimilar waveguides effectively keeps the spectrum from developing significant ripple until the waveguide separation (gap) is less than approximately 250 nm, showing a significant reduction in the minimal gap.

[0069] Experimental results for sample MZI devices will now be discussed. Michelson interferometer results will be discussed later in this disclosure. Five different MZI devices were fabricated to study the effect of dense dissimilar waveguide routing on the tuning efficiency of MZI switches. MZI Device 1 was used as a baseline device using identical waveguides and a gap of 3 μm to ensure no degradation of the spectrum due to crosstalk. MZI Devices 2 and 3 used dissimilar waveguide routing with a gap of 1 μm, and MZI devices 4 and 5 used dissimilar waveguides with a gap of 0.5 μm for the most dense routing. Table 1 summarizes the parameters of each MZI device. The widths of the waveguides were picked such that adjacent waveguides have a width difference of at least 100 nm and next-to-adjacent waveguides have a width difference of at least 50 nm to protect against any effect of non-nearest neighbor coupling that was not considered in the theoretical analysis. MZI device 1 was fabricated only in an unetched configuration while MZI devices 2-5 were fabricated in both unetched and underetched configurations. It is pointed out that the so called "unetched" MZI devices included isolation trenches at the sides, but were not etched underneath.

Table 1: Device parameters

	Device 1	Device 2	Device 3	Device 4	Device 5
N	3	5	5	9	9
w_i (nm)	500, 500 500	500, 400 550, 650 500	500, 400 550, 650 500	500, 600, 400 550, 650, 450 600, 400, 500	500, 600, 400 550, 650, 450 600, 400, 500
g (μm)	3.0	1.0	1.0	0.5	0.5
L (μm)	120	90	290	90	290

[0070] These MZI devices were subject to the following experimental procedure. A tunable laser source was used to inject 0 dBm of light through an optical fiber into the chip through transverse electric (TE) grating couplers. After passing through a device, the light exited the chip through a second fiber grating coupler and the transmitted light was passed to a photodetector. The wavelength of the input light was swept from 1530 nm to 1580 nm in 0.1 nm steps and the transmission spectrum of the device was recorded. This procedure was repeated while applying several different current levels to the phase shifter heaters and recording the power supplied.

[0071] In each case, the extinction ratio of the switch was measured to be greater than 20 dB. Figures 11A and 11B show example optical spectra of the underetched versions of MZI devices 3 and 5, respectively, in the on and off state. It can be seen that even for the longest devices tested, the more aggressive waveguide routing density of MZI device 5 compared to MZI device 3 did not have a negative effect on either the extinction ratio of the switch or the ripple in the transmission spectrum, which is maintained at below 0.1 dB peak to peak. This suggests that the dissimilar waveguides have successfully prevented cross-coupling of power in the dense routing regions of the switch. The insertion losses of the switches were estimated to be -0.9 dB, -1 dB, -2.5 dB, -1.2 dB, and -2.9 dB for devices 1-5, respectively. The difference in insertion loss is due to the difference in propagation loss for the different arm path lengths. The insertion loss was found not to depend on whether or not the device was underetched. The envelope of the transmission spectrum in the on state is due to the wavelength-dependent coupling efficiency of the grating couplers used. The wavelength dependence of the extinction ratio is due to an optical length mismatch between the two arms, which is likely due to variations in the thickness of the silicon layer across the wafer. The period of the variations in the extinction ratio could be extended to create a more broadband device by designing a switch such that the average distance between its arms is smaller, at the expense of an increased thermal crosstalk between the arms.

[0072] Figures 12A-D show the normalized transmission functions of the unetched and underetched versions of devices 2-5 as functions of the power applied to the thermal phase shifter, along with sinusoidal fits to the data. The wavelength of operation was 1550 nm. It can be seen that in many cases the devices with denser waveguide routing give higher phase shifter efficiency. Figure 12A illustrates normalized transmission functions of the short (devices 2 and

4) unetched MZI switches. Figure 12B illustrates normalized transmission functions of the long (devices 3 and 5) unetched MZI switches. Figure 12C illustrates normalized transmission functions of the short underetched MZI switches. Figure 12D illustrates normalized transmission functions of the long underetched MZI switches.

Table 2: Tuning efficiency of MZI switches

	Device 1	Device 2	Device 3	Device 4	Device 5
Unetched	14 mW/π	8.7 mW/π	5.9 mW/π	3.8 mW/π	4.2 mW/π
Underetched	N/A	0.68 mW/π	0.16 mW/π	0.20 mW/π	0.095 mW/π

[0073] Figures 13A-B show the temporal responses of the MZI switches when the heaters were driven with a square pulse. Temporal responses of Figure 13A were for unetched and Figure 13B for underetched MZI switches. The temporal response was found not to depend significantly on the waveguide routing density, but only on the heater length and whether or not the device was underetched. This suggests that the increase in device efficiency with increasing waveguide density does not come at the expense of a slower response time. The measured response times are summarized in Table 3. It is clear that the increases in efficiency when underetching devices or increasing device length come with an increase in the response time due to the improved thermal isolation of the heated region from its environment.

Table 3: Response times of MZI switches

	Unetched Short	Unetched Long	Underetched Short	Underetched Long
Rise Time (μs)	40	60	550	750
Fall Time (μs)	45	65	550	1200

[0074] Accordingly, increased waveguide routing density near a heating element is achievable by using dissimilar waveguides, which can be an effective way to improve the efficiency of thermal phase shifters. Utilizing highly dense routing of 9 waveguides under a 10 mm wide heater resulted in an MZI switch with ultra-low switching power of 95 mW while maintaining an extinction ratio greater than 20 dB and ripple in the through response of less than 0.1 dB. The waveguide routing density was found to not impact the switch response time.

[0075] Experimental/simulation results using example Michelson Interferometer Configuration (MIC) devices similar to that of Figure 4 will now be discussed.

[0076] Figure 14 shows the maximum optimal coupling for 1550 nm light between two dissimilar waveguides with widths of 400 nm, 500 nm, and 600 nm and thickness of 200nm. The simulation results are calculated using Mode Solutions. As can be seen from Figure 14, a maximum coupling of less than -30 dB can be obtained for gaps larger than 400 nm.

[0077] The phase shift $\Delta\varphi$ of the switch can be expressed as:

$$\Delta\varphi = \frac{2\pi}{\lambda}\frac{dn}{dT}\Delta T\, 2NL \qquad (18)$$

where $\frac{dn}{dT} = 1.86\times10^{-4}K^{-1}$ is the thermo-optic coefficient of Si and ΔT is the temperature difference between the two arms. N is the number of parallel waveguide sections as shown in Figure 6. λ is the wavelength. L is the length of the heater, i.e. 249μm in this embodiment. The Michelson Interferometer Configuration contributes to the phase tuning efficiency by a factor of 2; the thermal isolation of the suspended phase tuning arm contributes to a higher ΔT; the dense folded waveguide contributes to the phase tuning by a factor of N.

[0078] A series of MCI test devices were fabricated, as shown in Table I:

TABLE I: List of the fabricated test devices

Device	N	Suspended	g (nm)	w_i (nm)	$2 \cdot N \cdot L$ (mm)
1	1	No	NA	w_1=500	0.498
2	1	Yes	NA	w_1=500	0.498
3	7	No	1000	$w_{1,4,7}$=500, $w_{2,5}$=600, $w_{3,6}$=400	3.486
4	7	Yes	1000	$w_{1,4,7}$=500, $w_{2,5}$=600, $w_{3,6}$=400	3.486
5	11	No	430	$w_{1,4,7,10}$=500, $w_{2,5,8,11}$=600, $w_{3,6,9}$=400	5.478
6	11	Yes	430	$w_{1,4,7,10}$=500, $w_{2,5,8,11}$=600, $w_{3,6,9}$=400	5.478

$2 \cdot N \cdot L$ is the optical interaction length with the heated region.

[0079] The test devices discussed herein were fabricated using a 248 nm process at the Institute of Microelectronics (IME), Singapore. Six different devices were fabricated on the same wafer to investigate the effects of the suspended phase arms and the densely folded waveguides on the tuning efficiency. Table 1 lists the parameters of the fabricated devices. MIC devices 1 and 2 do not use folded waveguides in their phase arms. MIC devices 3 and 4 use N=7 folded waveguides with waveguide gaps of 1 μm. MIC devices 5 and 6 use N=11 folded waveguides with smaller waveguide gaps of 430 nm. On chip grating couplers [22] were used to couple light into an out of the test devices. A pair of grating couplers connected by a short waveguide was also fabricated for calibrating the insertion loss.

[0080] To characterize these devices, a polarization maintaining fiber array was used to align with the input/output grating couplers. An Agilent 81600B tunable laser was used as the optical input source, an Agilent 81635A optical power sensor was used as the optical output detect, and a Keithley 2602A dual-channel system source meter was used as the electrical power source for thermal tuning.

[0081] The measured resistances of the metal heaters are approximately 380 Ω for all devices. Figure 15A presents the TE mode transmission at switching ON and OFF states for MIC test device 6. For the same device, the measured insertion loss is 3.3 dB at 1550 nm, which is mainly due to the round-trip propagation loss of the 4.27 mm long phase arms and the waveguide bends. As shown in Figure 15B, at 1550 nm the measured power to switch from the maximum to minimum transmission is 50 μW, and the switching extinction ratio is 26 dB. Figure 15C shows the 10%-90% response time for MIC device 6 is 1.28 ms, including a 780 μs rise time and a 500 μs fall time.

[0082] For comparison, measurement results for all test devices are shown in Figures 16A and 16B. As shown in Figure 16A, the power consumption of the devices significantly decreases when increasing the number of folds N in the waveguide, which is consistent with expectations from equation (18) above. To be clear, there are N parallel portions of the waveguide, with N-1 bends.

[0083] When comparing the devices with suspended structures to those without, the suspended structures demonstrated $1/35^{th}$ of the previous consumption. As shown in Figure 16B, increasing the number of waveguides does not significantly influence the response time of the devices. However, the response time of the devices with suspended structures is approximately 6 times slower than that of those without. For thermally isolated structures, there is a tradeoff between efficiency and response time, however the improvement in efficiency (35x) will likely be worth the degradation of response time (6x) for many applications.

[0084] Further improvements can be made to further reduce the power consumption according to some embodiments. Figure 17 shows a simulated 3D temperature distribution in the suspended arm of MIC device 6 when a power of 50 μW is supplied to the heater. This simulation has been obtained through a 3D heat transfer simulation. The two ends of the arm and the small support bridges between the isolation trenches have been found to be the major outlets of leaking heat. As a result, having a longer suspended arm and fewer bridges may improve thermal isolation, and thus further reduce the power consumption of the switches. Additionally, thermal isolation can be applied to the second arm of the interferometer to further reduce the thermal crosstalk between the arms.

[0085] Accordingly, photonic ultra-efficient thermo-optic switches on a 220 nm silicon-on-insulator (SOI) platform have been demonstrated. Folded waveguides in a Michelson Interferometer Configuration can be used to increase the optical interaction length of the light with the heated region, and a suspended structure can be used to improve thermal isolation. An ultra-low switching power of 50 μW is realized with an extinction ratio of over 26 dB for the transverse electric (TE) mode at 1550 nm. The 10%-90% response time of the switch is 1.28 ms, including a 780 μs rise time and a 500 μs fall time. These results demonstrate a significant reduction in power consumption compared to prior art devices.

[0086] It should be appreciated that the techniques suggested herein can be extended to other switching architectures where low power switching is desired.

[0087] Although the present disclosure has been described with reference to specific features and embodiments thereof, it is evident that various modifications and combinations can be made thereto without departing from the disclosure. The specification and drawings are, accordingly, to be regarded simply as an illustration of the disclosure as defined by the appended claims, and are contemplated to cover any and all modifications, variations, combinations or equivalents that fall within the scope of the present disclosure.

Claims

1. An optical device comprising:

first and second waveguide phase arms each having optically coupled parallel sections of waveguides, the parallel sections of each one of the first and second waveguide phase arms being dissimilar to lessen crosstalk; and

a tunable element for applying a phase shift to an optical signal traversing the first waveguide phase arm.

2. The optical device as claimed in claim 1 wherein each optically coupled parallel section of waveguides forms a single lightpath.

3. The optical device as claimed in claim 2 wherein the waveguides of the parallel sections have dissimilar dimensions.

4. The optical device as claimed in claim 2 wherein adjacent waveguides of the parallel sections vary in one or more of gap, width, and/or thickness.

5. The optical device as claimed in claim 4 wherein the first and second waveguide phase arms comprise a plurality of tapered waveguides of different dimensions which are connected by loops, and the loops form transitions between the different dimensions.

6. The optical device as claimed in claim 5 wherein there are N parallel sections and N-1 loops, with N being an odd integer greater than or equal to 3, such that input and output signals in each one of the first and second waveguide phase arms travel in a same direction.

7. The optical device as claimed in claim 4 wherein the tunable element comprises a thermo-optic heater thermally coupled to the first waveguide phase arm.

8. The optical device as claimed in claim 7 wherein the optical device is a silicon photonic device, and wherein the thermo-optic heater comprises a metallic layer.

9. The optical device as claimed in claim 7 wherein the first waveguide phase arm is suspended for better thermal isolation thereof.

10. The optical device as claimed in claim 8 wherein the optical device in the region of the thermo-optic heater is underetched to improve thermal isolation of the first waveguide phase arm adjacent the thermo-optic heater.

11. The optical device as claimed in claim 4 further comprising a coupler configured as both an input power splitter for splitting an input optical signal between the first and second waveguide phase arms, and as an output power combiner for recombining optical signals from the first and second waveguide phase arms to produce an output optical signal.

12. The optical device as claimed in claim 11 wherein the optical device is configured as a Michelson interferometer, and wherein the first and second waveguide phase arms are terminated with waveguide reflectors at ends of the first and second waveguide phase arms.

13. The optical device as claimed in claim 12 wherein the one or more couplers comprise a 2x2 coupler selected from a group consisting of an adiabatic coupler, a multimode interference (MMI) coupler, and a directional coupler.

14. The optical device as claimed in claim 12 wherein the waveguide reflectors comprise loop mirrors.

15. The optical device as claimed in claim 14 wherein the loop mirror comprises a compact Y-branch and a bent waveguide.

16. The optical device as claimed in claim 4 wherein the optical device is configured as a thermo-optic switch.

17. The optical device as claimed in claim 16 further comprising one or more couplers configured as input power splitters for splitting an input optical signal between the first and second waveguide phase arms, or as output power combiners for recombining the

optical signal from the first and second waveguide phase arms to produce an output optical signal.

18. The optical device as claimed in claim 17 wherein the optical device is configured as a tunable Mach-Zehnder interferometer based optical switch.

19. The optical device as claimed in claim 18 wherein the optical device is configured as a modulator.

20. The optical device as claimed in claim 2 wherein the optical device is configured as a tunable Mach-Zehnder interferometer wherein at least adjacent waveguides of the parallel sections have varying widths.

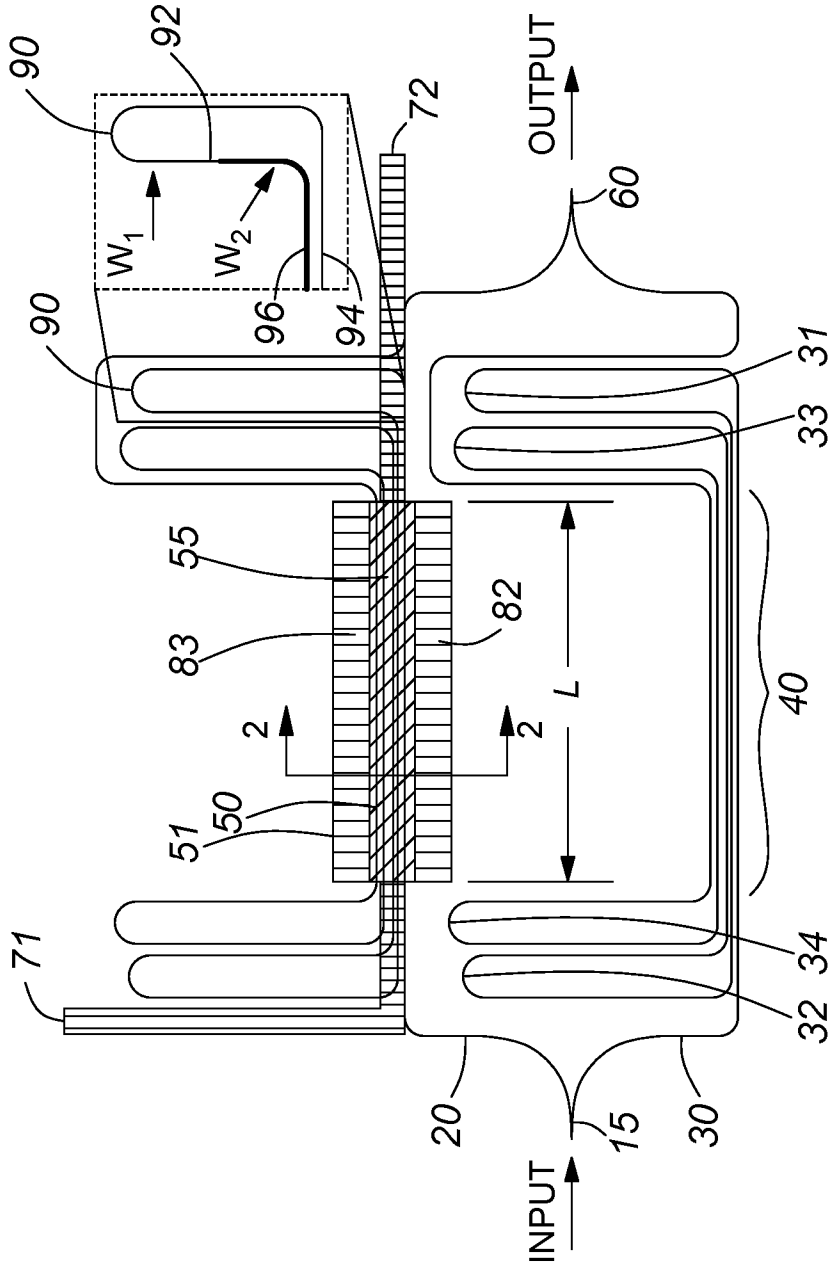
90
92
72
OUTPUT
60
W_1
W_2
96
94
90
31
33
55
82
83
2
2
L
40
50
51
71
34
32
20
15
30
INPUT

FIG. 1

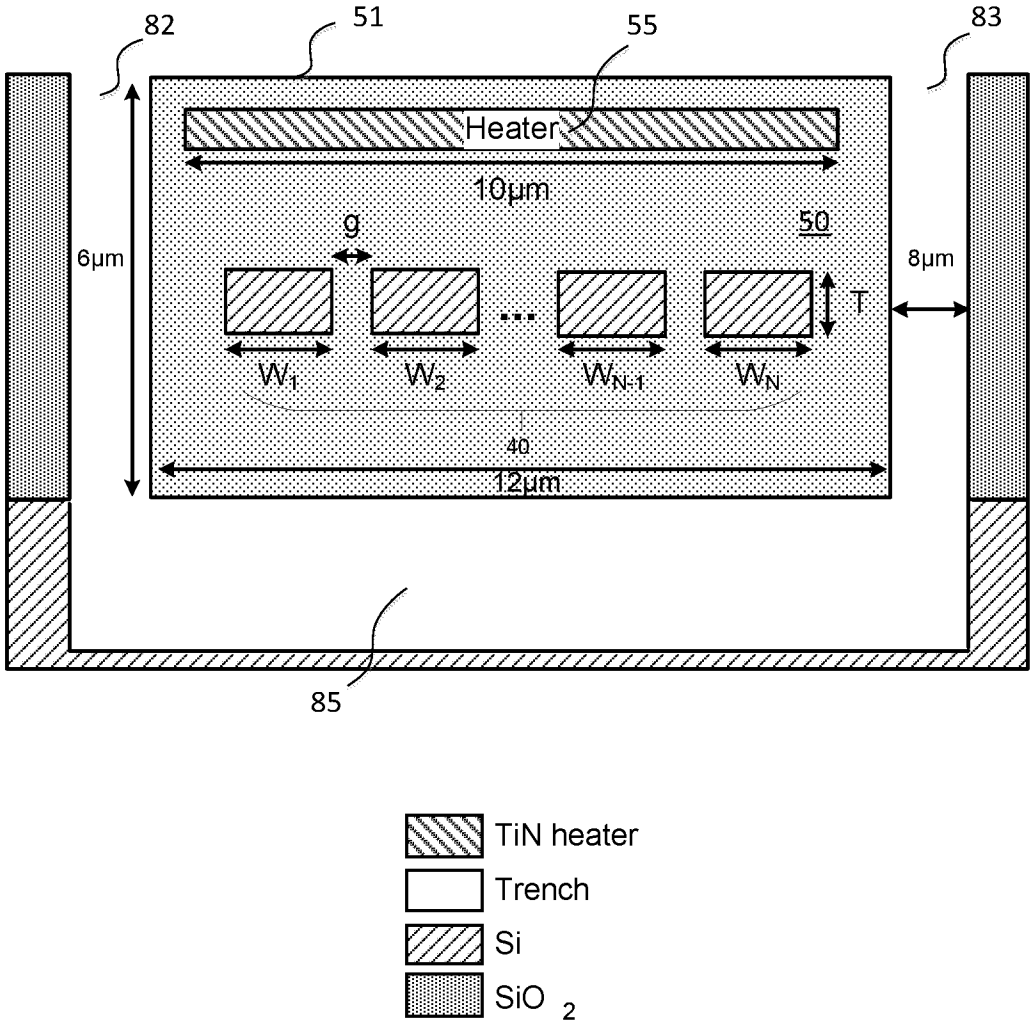
82
51
55
83
Heater
10μm
g
50
6μm
8μm
T
W1
W2
WN-1
WN
40
12μm
85
TiN heater
Trench
Si
SiO 2

FIG 2

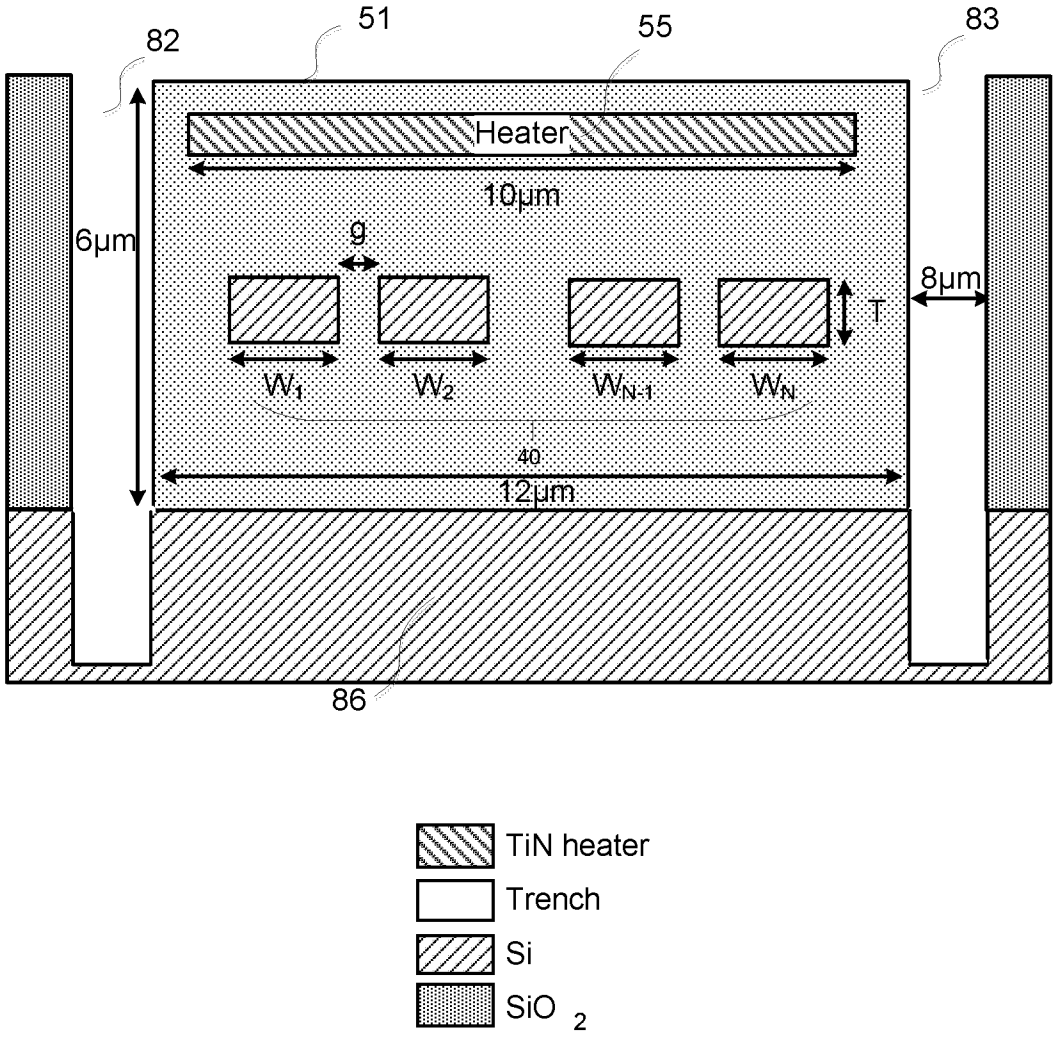
82
51
55
83
Heater
10μm
6μm
g
8μm
T
W1
W2
WN-1
WN
40
12μm
86
TiN heater
Trench
Si
SiO 2

FIG 3

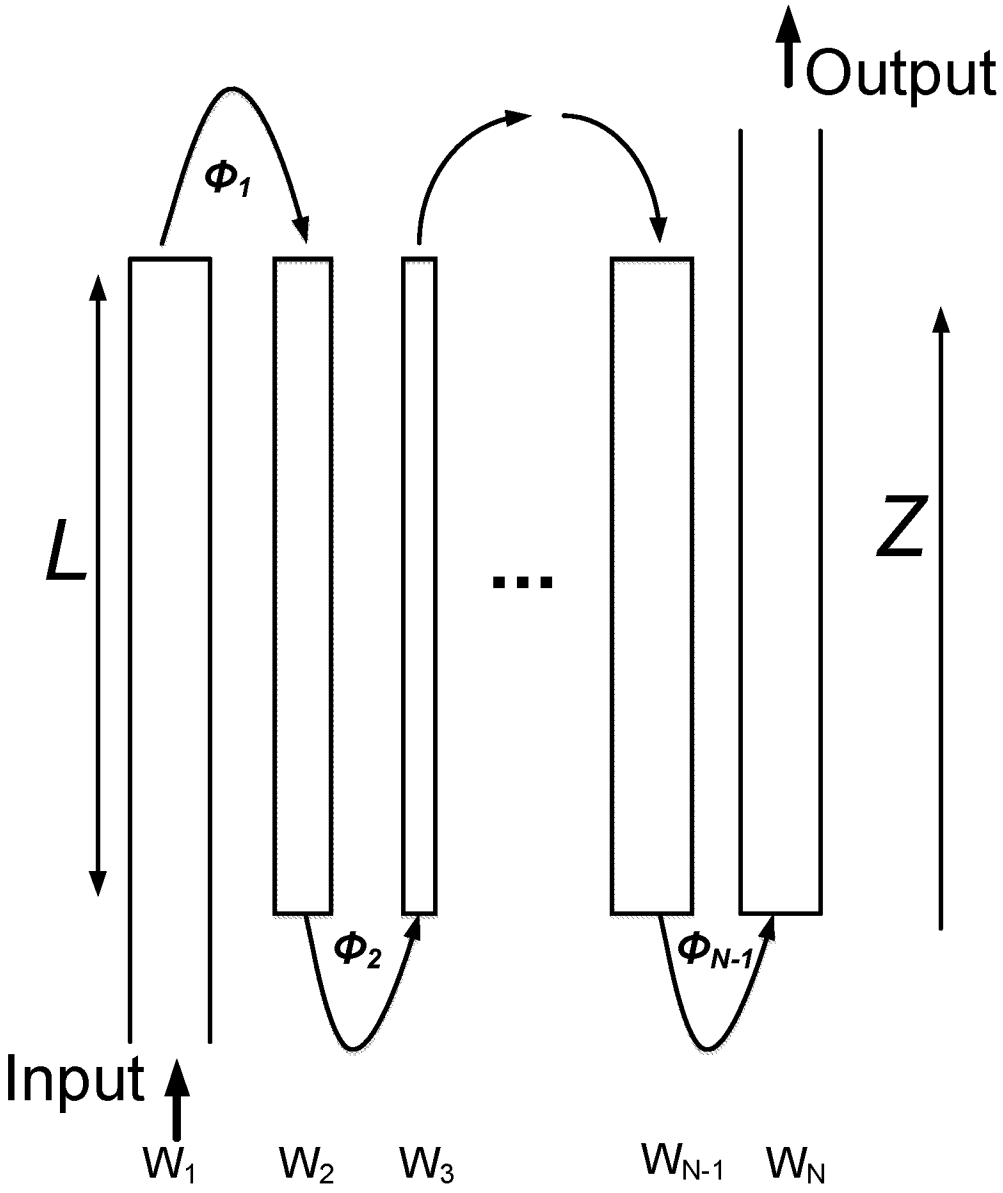

FIG 4

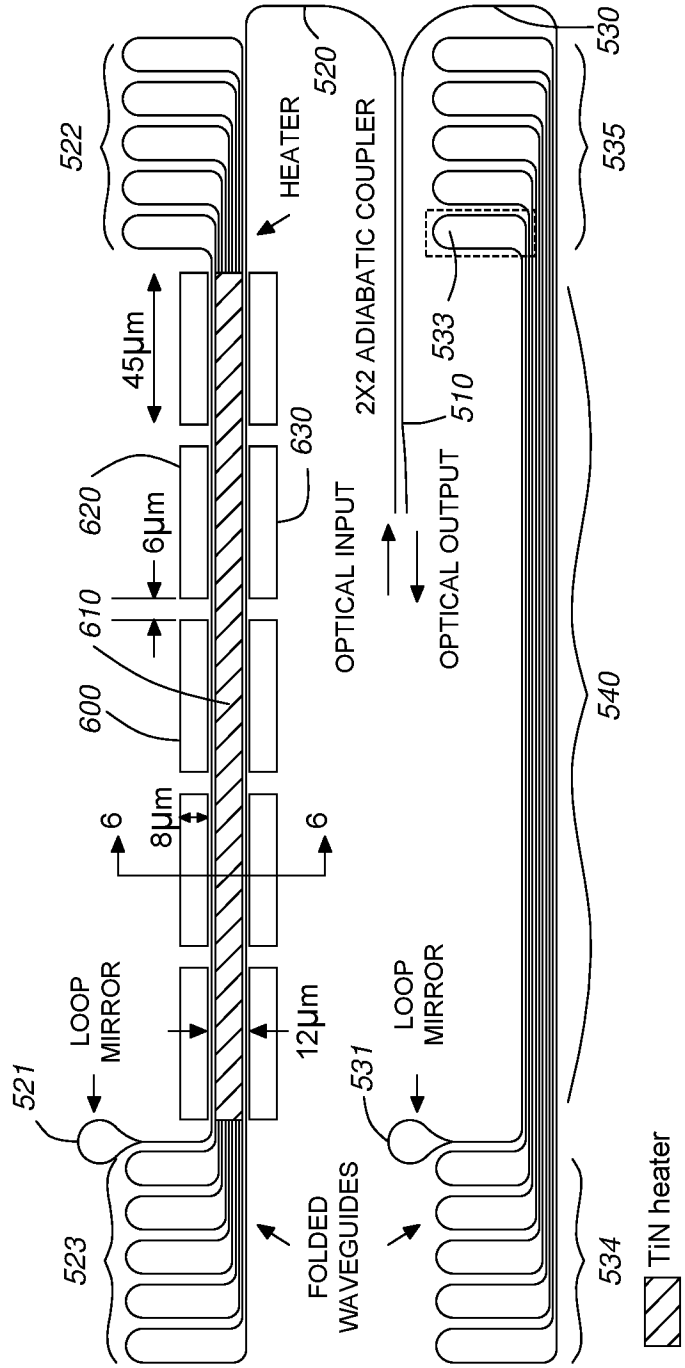
522
520
HEATER
530
535
45μm
630
620
6μm
610
600
8μm
6
6
2X2 ADIABATIC COUPLER
533
510
OPTICAL INPUT
OPTICAL OUTPUT
540
LOOP MIRROR
521
12μm
LOOP MIRROR
531
FOLDED WAVEGUIDES
523
534
TiN heater

FIG. 5

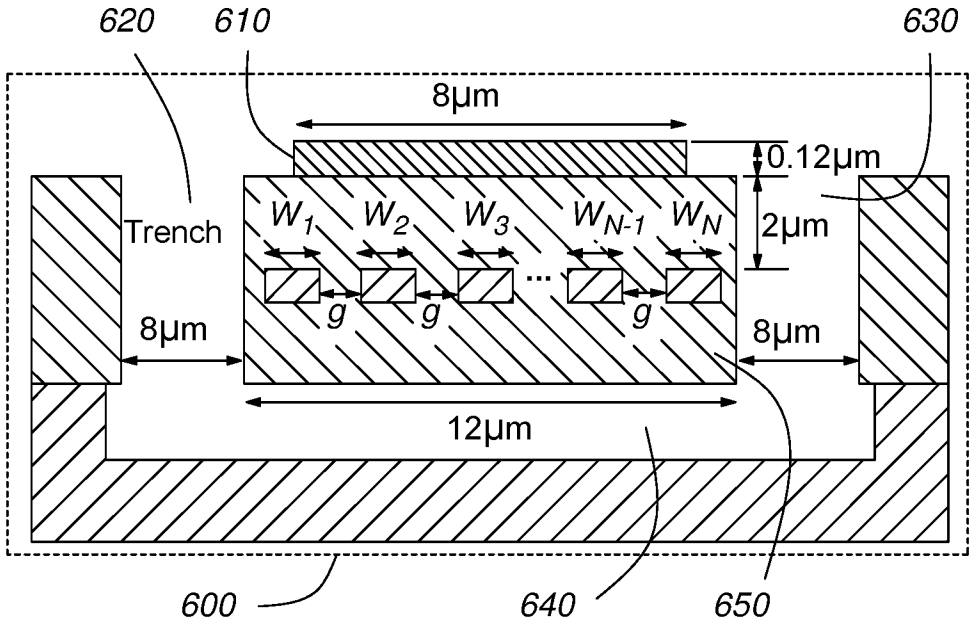
620
610
630
8μm
0.12μm
Trench
W_1
W_2
W_3
W_{N-1}
W_N
2μm
g
g
g
8μm
8μm
12μm
600
640
650
TiN heater
Trench
Si
SiO 2

FIG. 6

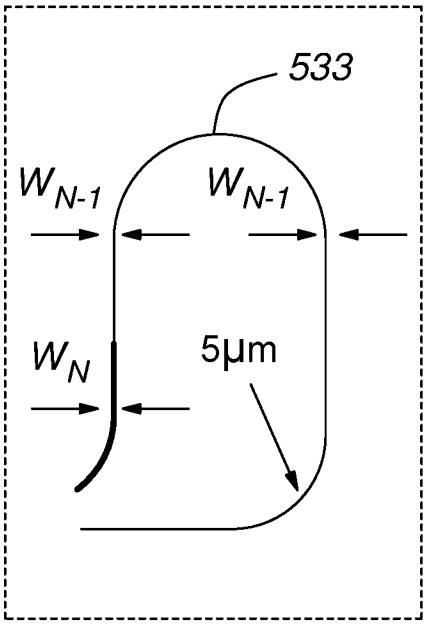

FIG. 7

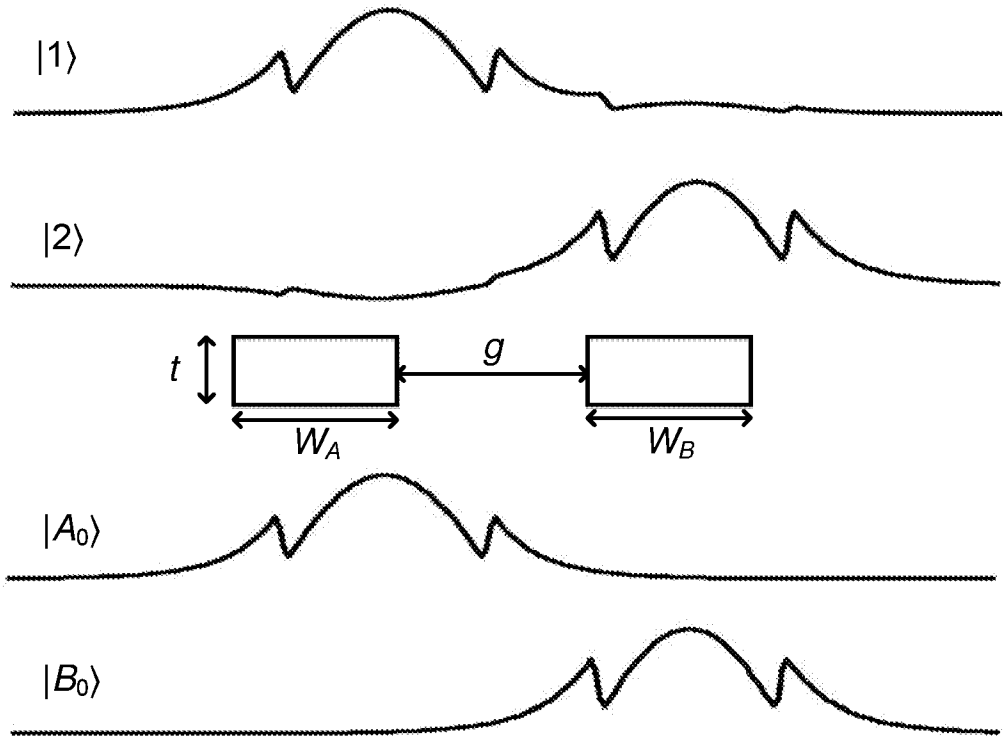

FIG 8

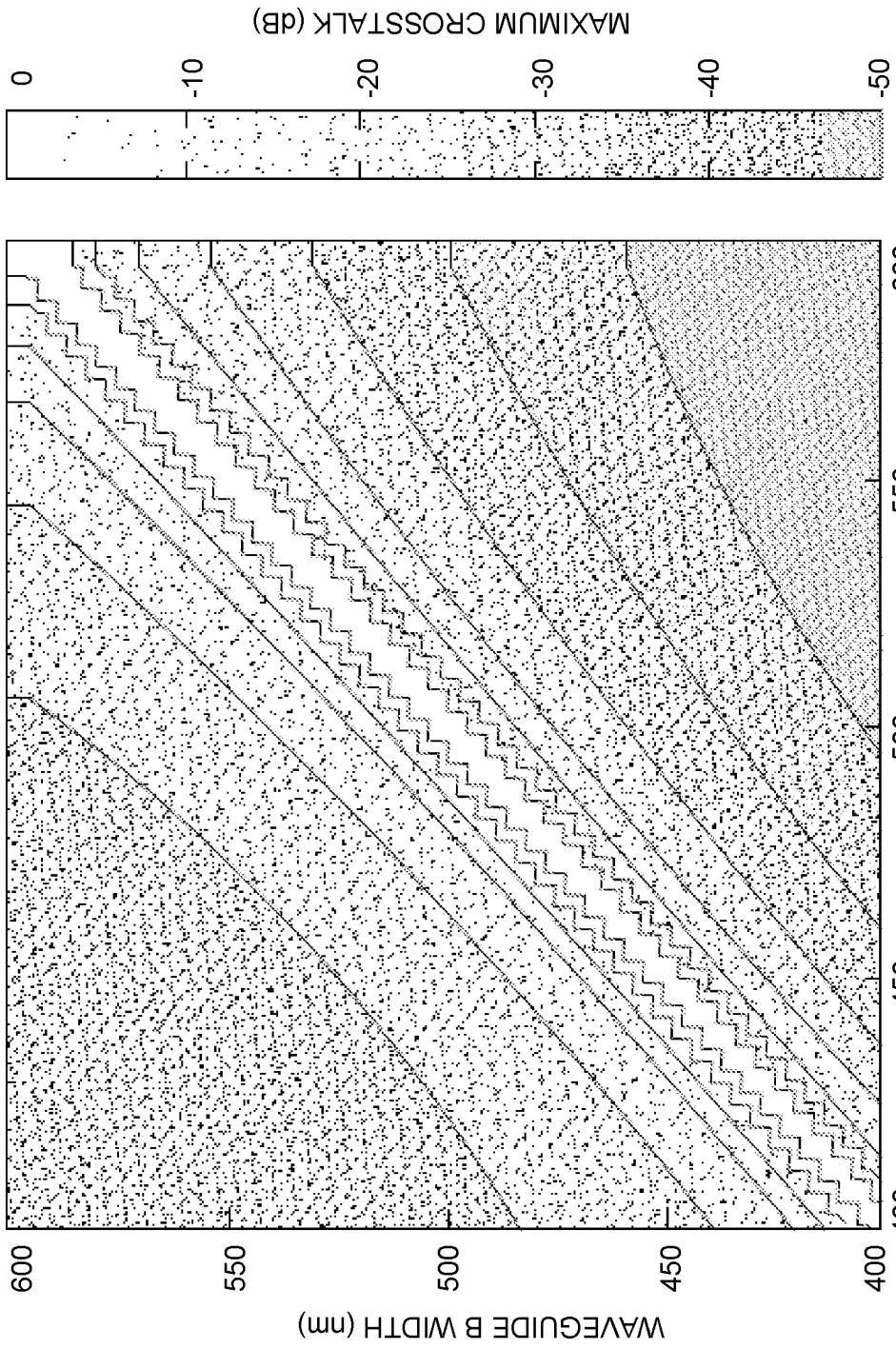
MAXIMUM CROSSTALK (dB)
0
-10
-20
-30
-40
-50
WAVEGUIDE B WIDTH (nm)
600
550
500
450
400
WAVEGUIDE A WIDTH (nm)
400
450
500
550
600

FIG. 9

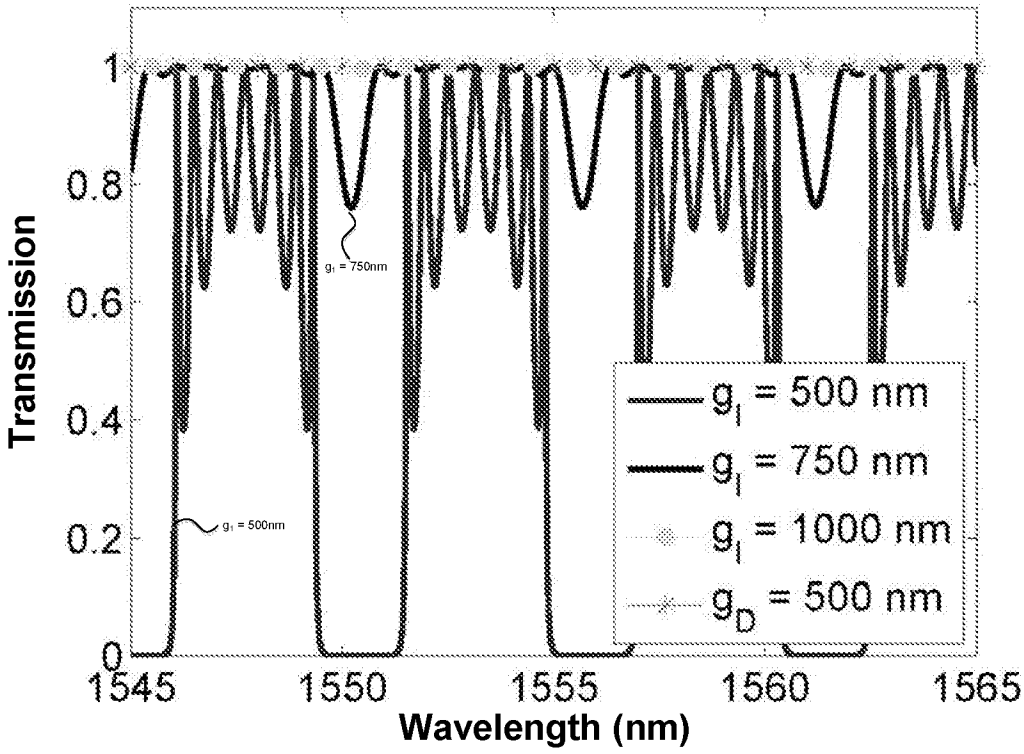
Transmission
1
0.8
0.6
0.4
0.2
0
1545
1550
1555
1560
1565
Wavelength (nm)
g1 = 750nm
g1 = 500nm
g1 = 500 nm
g1 = 750 nm
g1 = 1000 nm
gD = 500 nm

FIG 10A

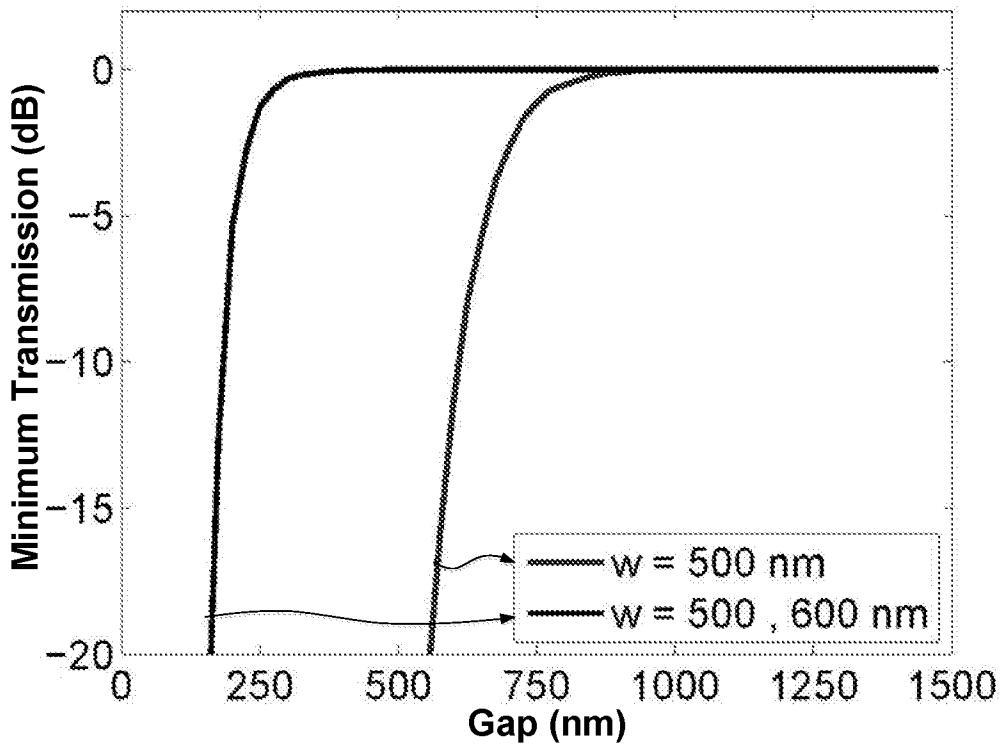
Minimum Transmission (dB)
0
−5
−10
−15
−20
0
250
500
750
1000
1250
1500
Gap (nm)
w = 500 nm
w = 500 , 600 nm

FIG 10B

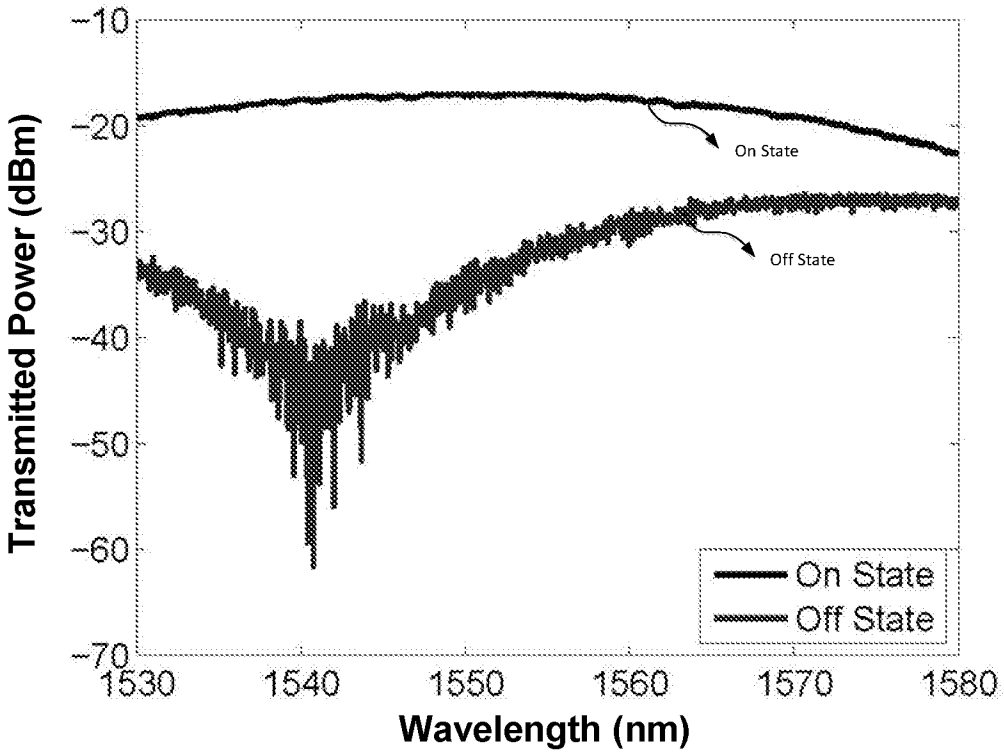
−10
−20
−30
−40
−50
−60
−70
Transmitted Power (dBm)
On State
Off State
On State
Off State
1530
1540
1550
1560
1570
1580
Wavelength (nm)

FIG 11A

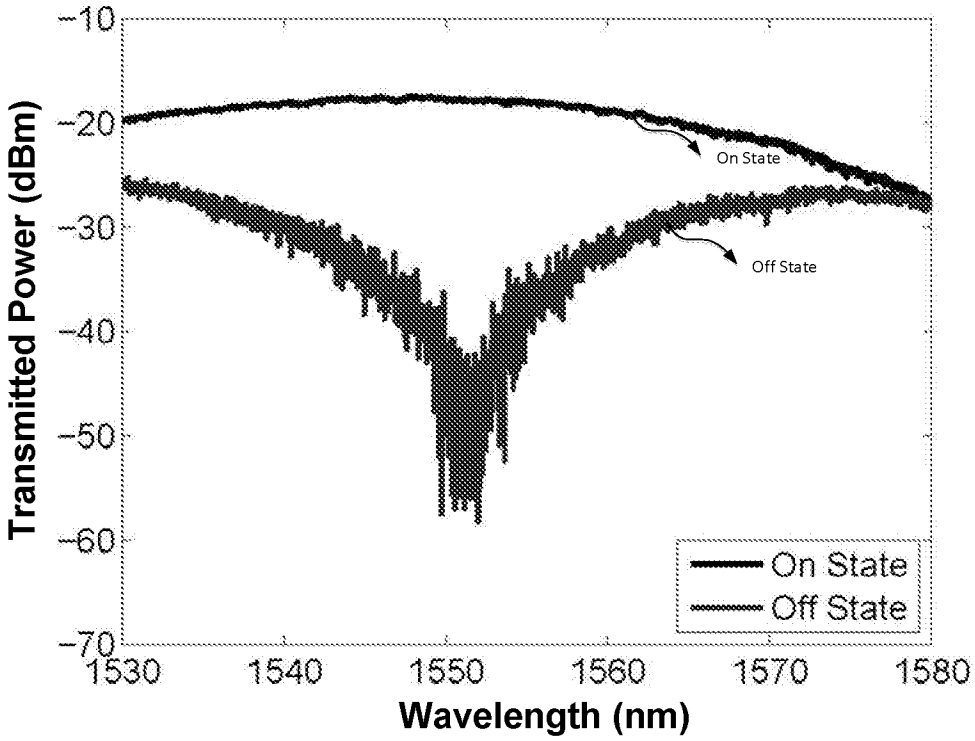
−10
−20
−30
−40
−50
−60
−70
Transmitted Power (dBm)
1530
1540
1550
1560
1570
1580
Wavelength (nm)
On State
Off State
On State
Off State

FIG 11B

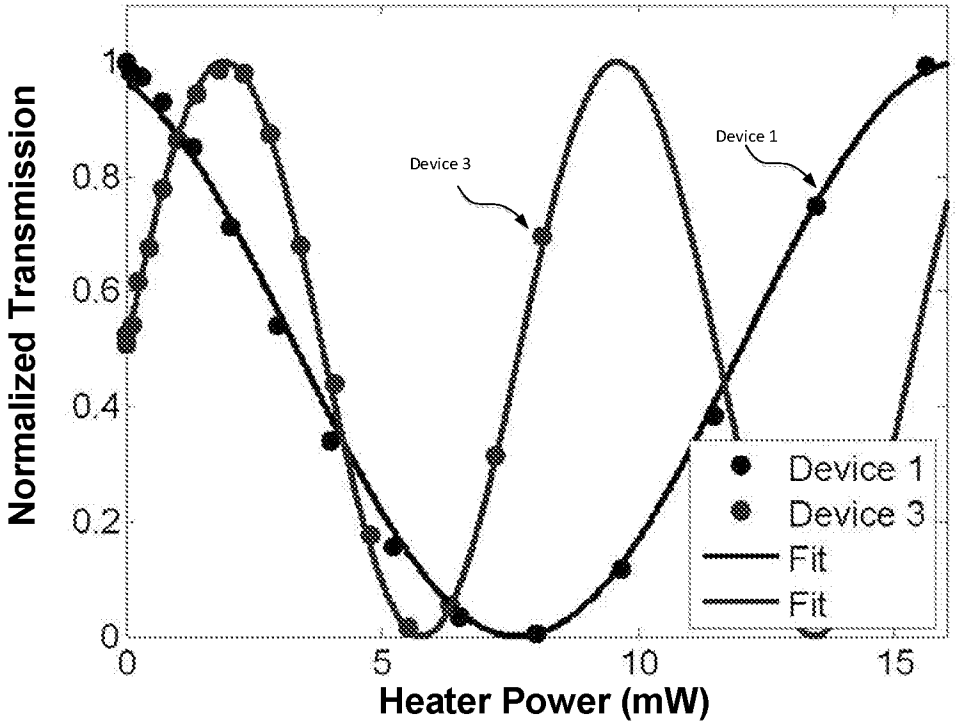
Normalized Transmission
Heater Power (mW)
Device 3
Device 1
Device 1
Device 3
Fit
Fit
0
0.2
0.4
0.6
0.8
1
0
5
10
15

FIG 12A

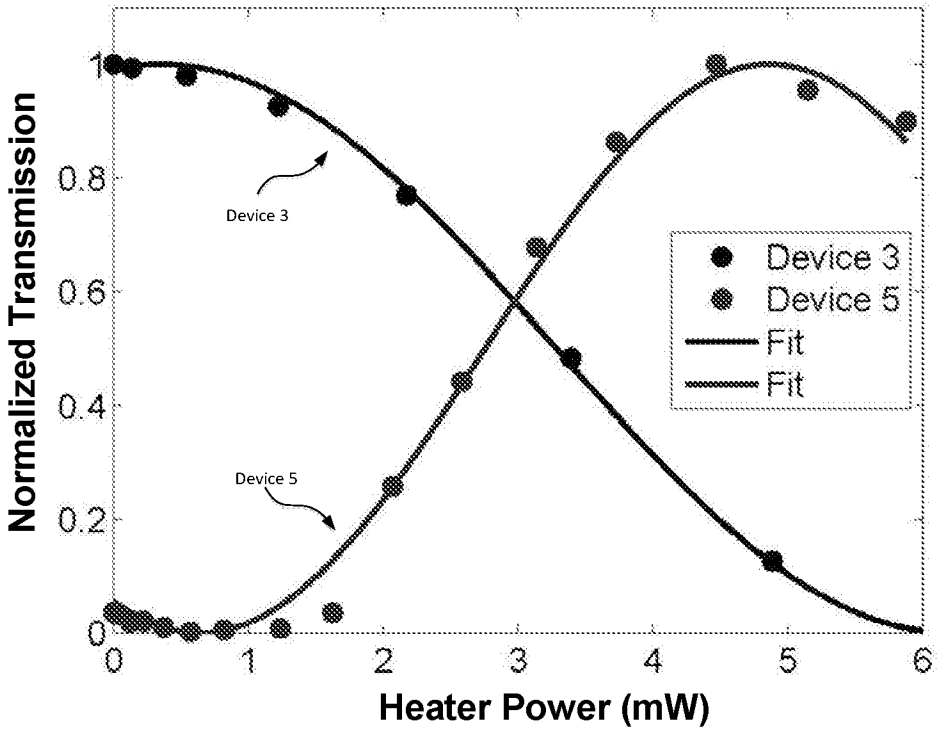
Normalized Transmission
Heater Power (mW)
Device 3
Device 5
Device 3
Device 5
Fit
Fit
0
0.2
0.4
0.6
0.8
1
0
1
2
3
4
5
6

FIG 12B

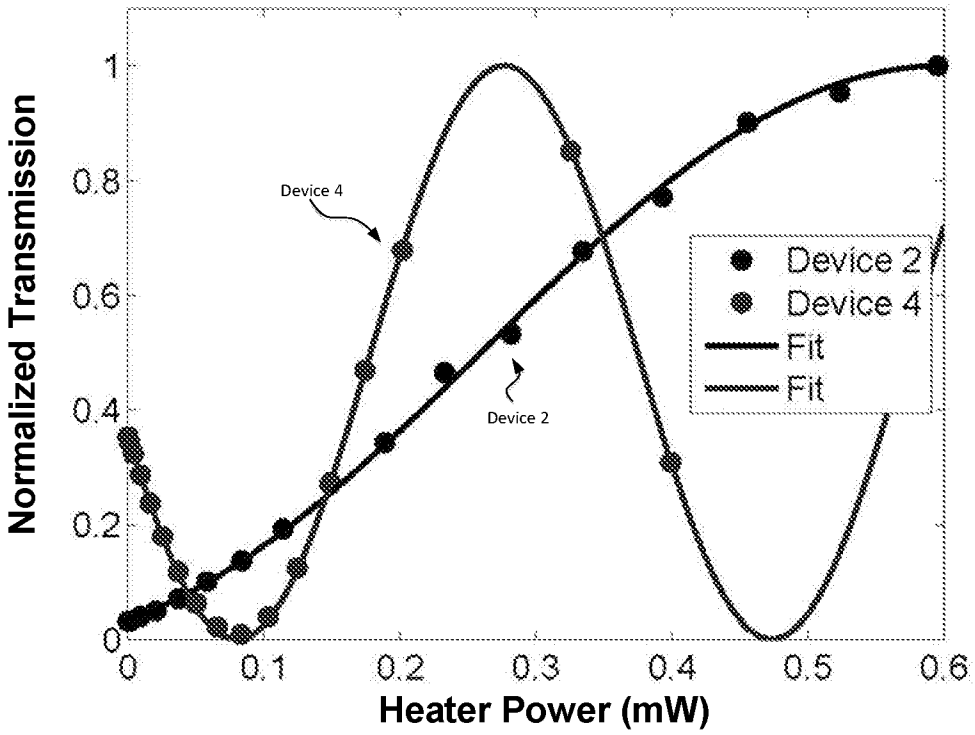
Normalized Transmission
Heater Power (mW)
Device 4
Device 2
Device 2
Device 4
Fit
Fit
0
0.2
0.4
0.6
0.8
1
0
0.1
0.2
0.3
0.4
0.5
0.6

FIG 12C

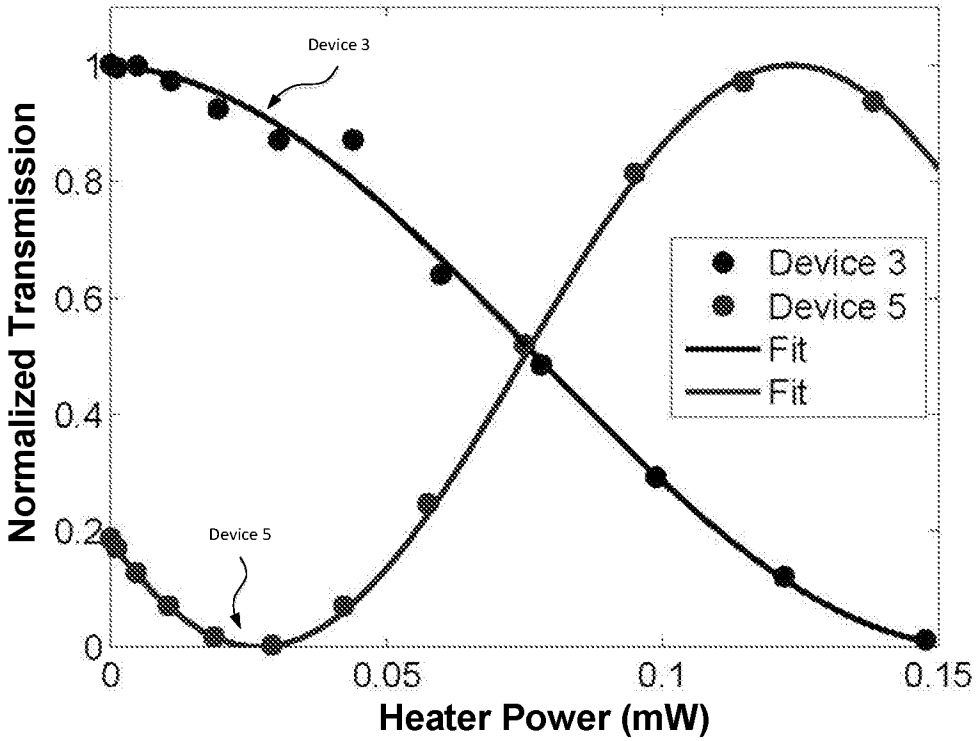
Device 3
Device 5
Normalized Transmission
Heater Power (mW)
Device 3
Device 5
Fit
Fit
0
0.2
0.4
0.6
0.8
1
0
0.05
0.1
0.15

FIG 12D

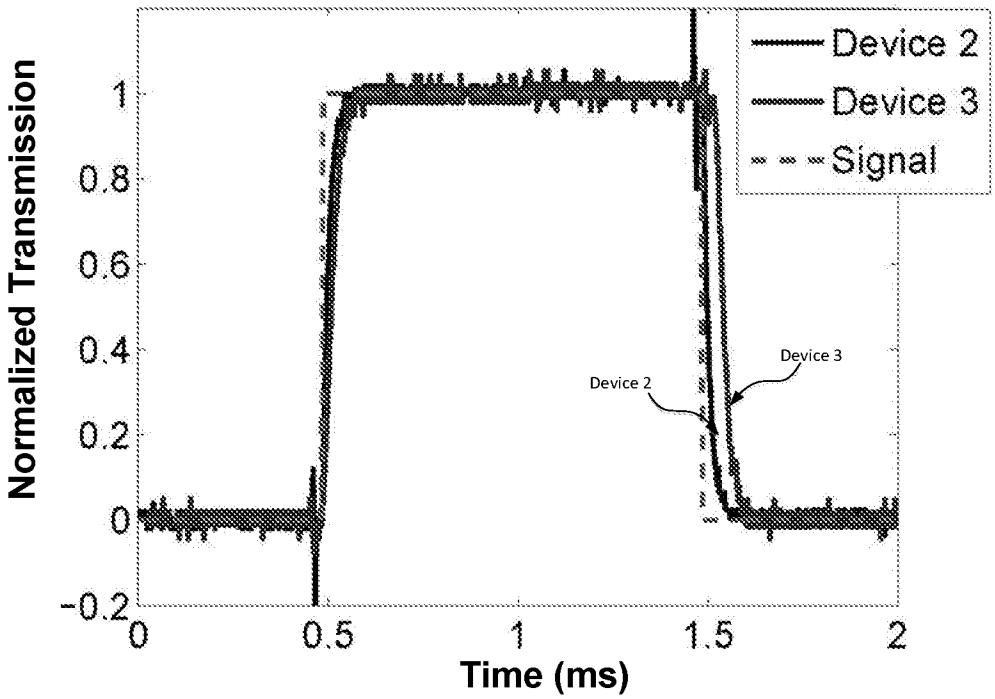
Device 2
Device 3
Signal
Normalized Transmission
1
0.8
0.6
0.4
0.2
0
-0.2
0
0.5
1
1.5
2
Time (ms)
Device 2
Device 3

FIG 13A

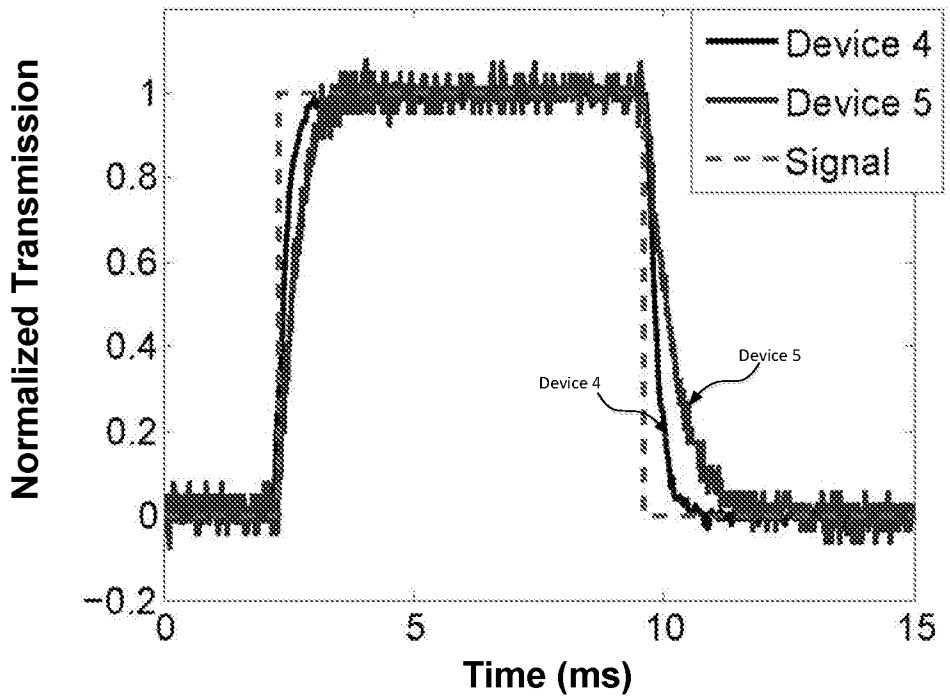
Normalized Transmission
1
0.8
0.6
0.4
0.2
0
−0.2
0
5
10
15
Time (ms)
Device 4
Device 5
Signal
Device 4
Device 5

FIG 13B

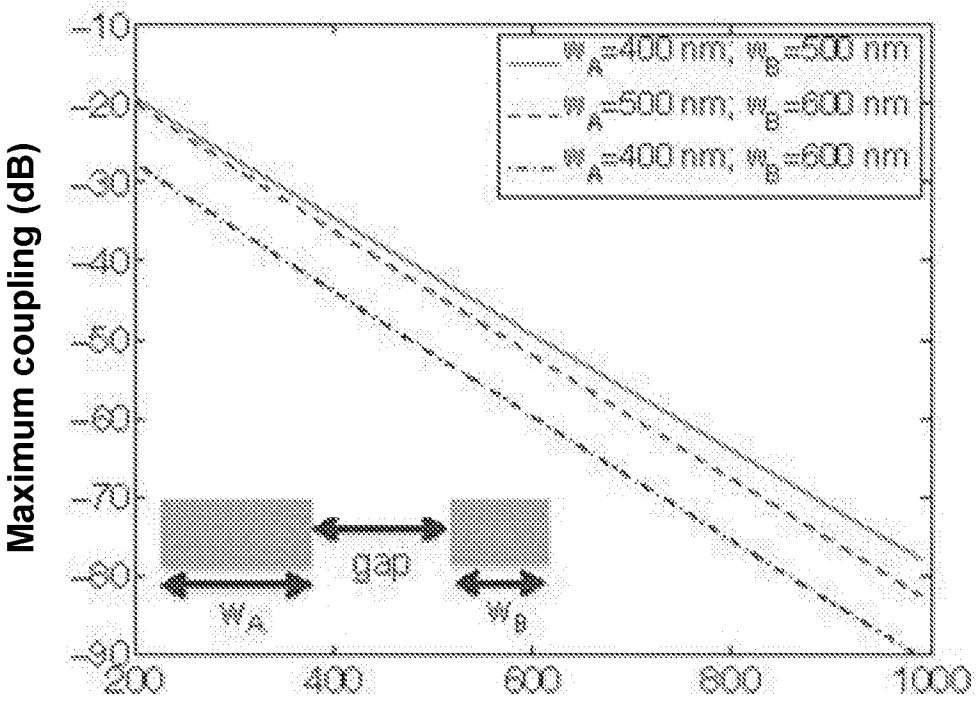
Maximum coupling (dB)
-10
-20
-30
-40
-50
-60
-70
-80
-90
200
400
600
800
1000
Gap (nm)
w_A=400 nm; w_B=500 nm
w_A=500 nm; w_B=600 nm
w_A=400 nm; w_B=600 nm
gap
w_A
w_B

FIG 14

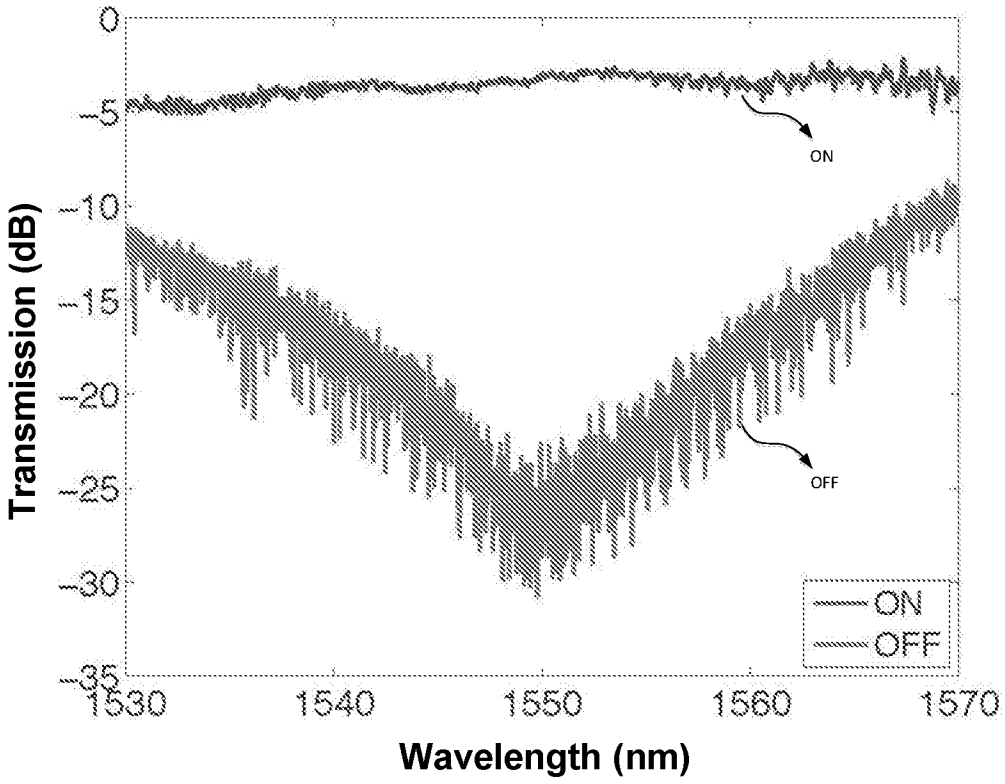
0
−5
−10
−15
−20
−25
−30
−35
Transmission (dB)
1530
1540
1550
1560
1570
Wavelength (nm)
ON
OFF
ON
OFF

FIG 15A

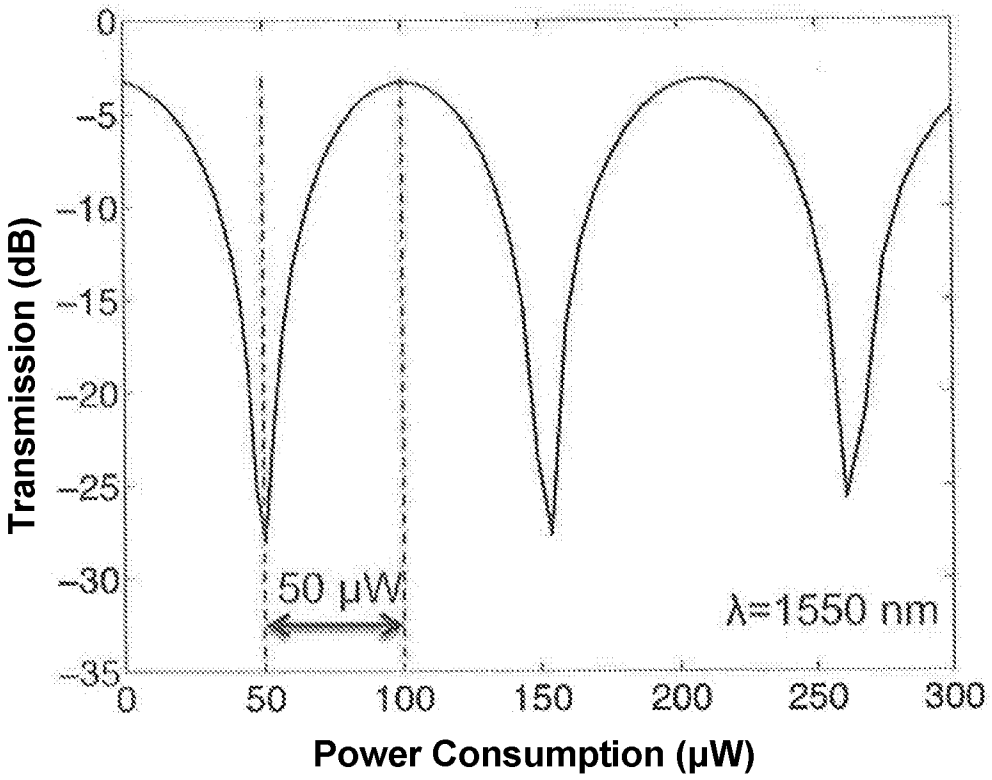
0
-5
-10
-15
-20
-25
-30
-35
Transmission (dB)
50 μW
λ=1550 nm
0
50
100
150
200
250
300
Power Consumption (μW)

FIG 15B

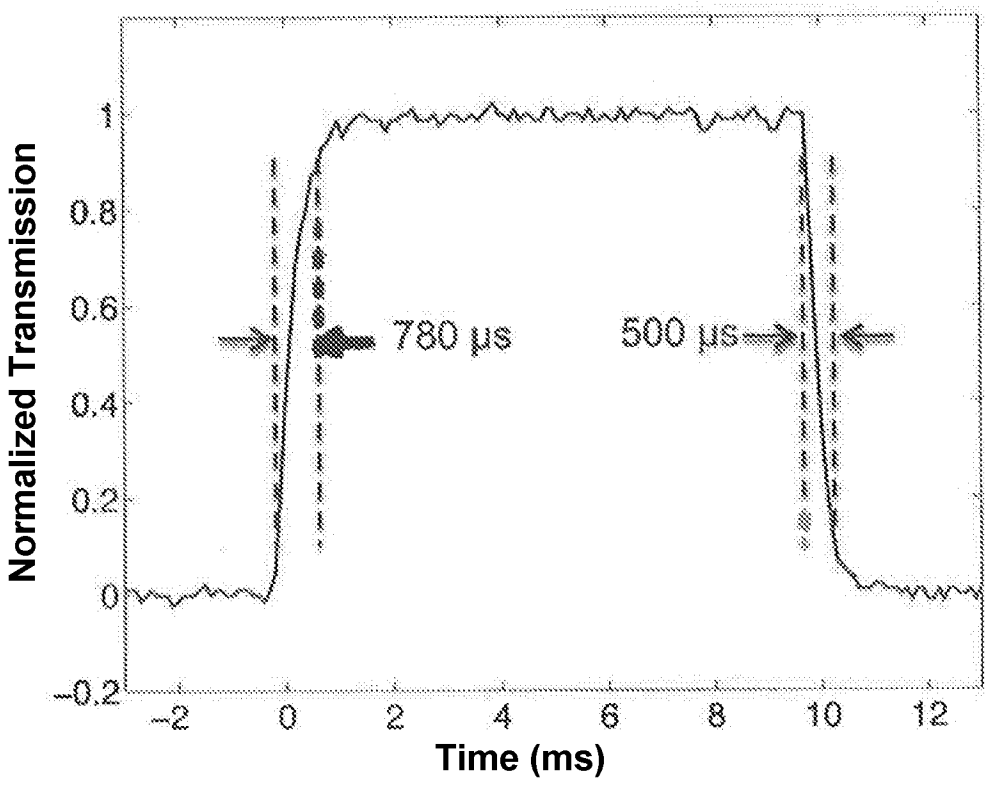
Normalized Transmission
1
0.8
0.6
0.4
0.2
0
-0.2
780 µs
500 µs
-2
0
2
4
6
8
10
12
Time (ms)

FIG 15C

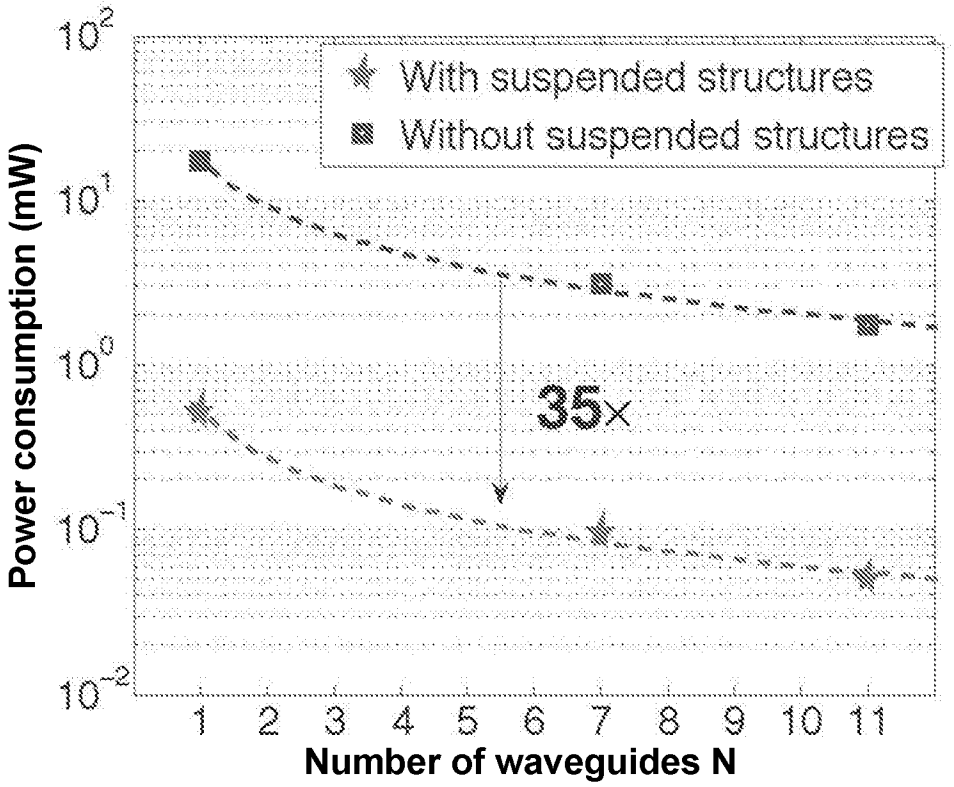
With suspended structures
Without suspended structures
35×
Power consumption (mW)
Number of waveguides N
10^2
10^1
10^0
10^-1
10^-2
1 2 3 4 5 6 7 8 9 10 11

FIG 16A

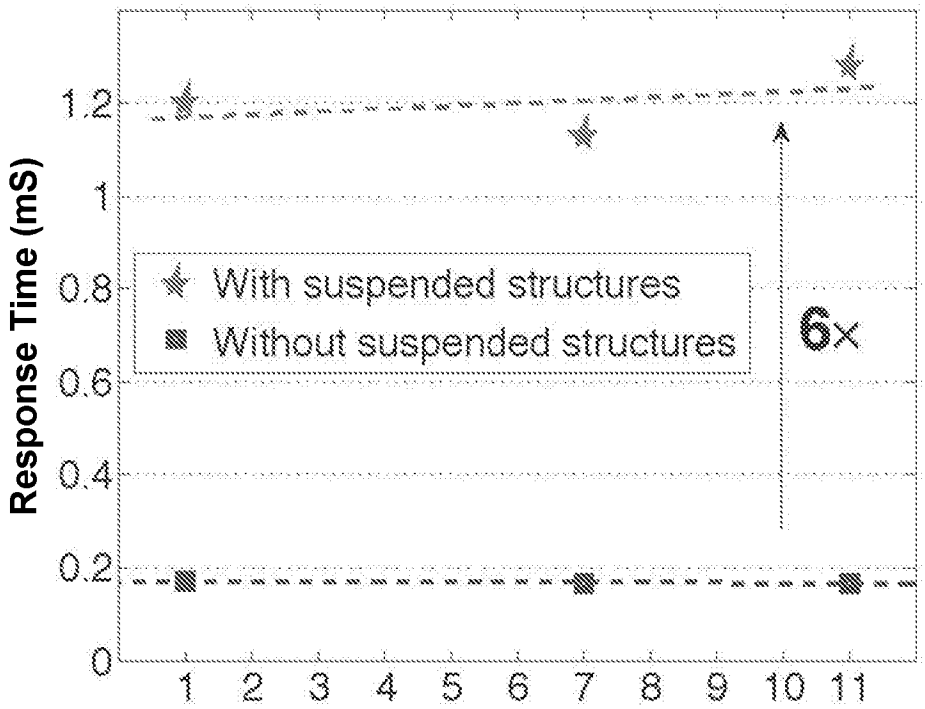
Response Time (mS)
1.2
1
0.8
0.6
0.4
0.2
0
With suspended structures
Without suspended structures
6×
1 2 3 4 5 6 7 8 9 10 11
Number of waveguides N

FIG 16B

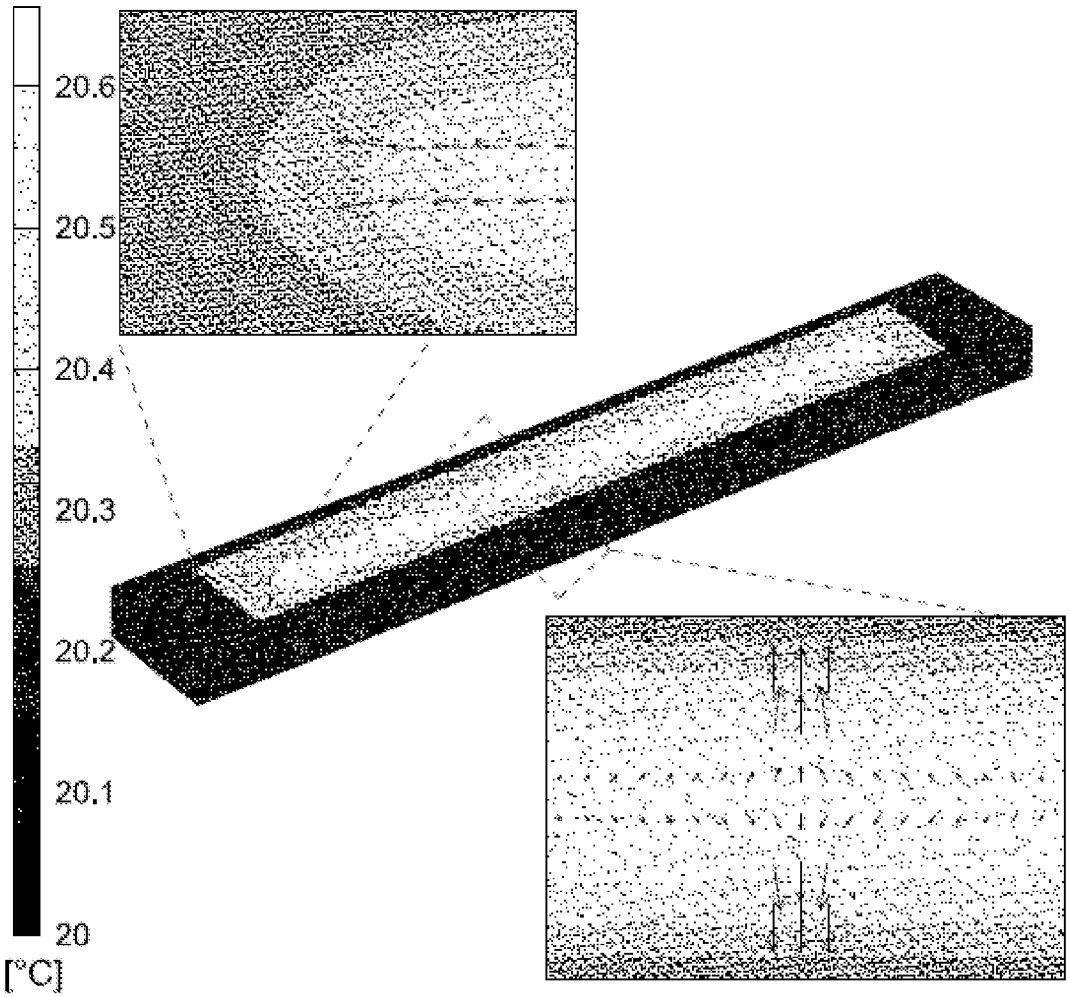

FIG. 17

INTERNATIONAL SEARCH REPORT

International application No.
PCT/CN2016/081533

A. CLASSIFICATION OF SUBJECT MATTER

G02B 6/12(2006.01)i

According to International Patent Classification (IPC) or to both national classification and IPC

B. FIELDS SEARCHED

Minimum documentation searched (classification system followed by classification symbols)

G02B6

Documentation searched other than minimum documentation to the extent that such documents are included in the fields searched

Electronic data base consulted during the international search (name of data base and, where practicable, search terms used)

CNABS;TWABS;VEN;CNKI:(OR THERMO-OPTIC+, THERMOOPTIC+, ((OR THERMO+, THERMAL+) 2D (OR OPTIC+, LIGHT+,PHOTO+))) 3D (OR SWITCH+, MODULAT????, (ON 1W OFF), VALVE?, GATE?,ATTENUAT+), ((OR PHASE?, PHASING) 3D (OR SHIFT???, DELAY???, TUNE?, TUNABLE,TUNING, VARY???,VARIES,VARIABLE, CHANG+, MODULAT???, REGULAT???, MODIF???, RECTIF???, ADJUST????)), MACH-ZEHNDER, (Mach 1D Zehnder), M-Z, MZ, INTERFERENCE, INTERFEROMETER, INTERFEROMETRY, INTERFEROMETRIC????, (OR FOLD+, SUPERPOS +, OVERLAP????, PARALLEL+) 2D (OR WAVEGUIDE?, LIGHTGUID+,((OR LIGHT, WAVE, OPTIC+) 1D GUID+)), (OR WAVEGUIDE?, LIGHTGUID+,((OR LIGHT, WAVE, OPTIC+) 1D GUID+)) 3D (OR VARY+, VARIABLE+, DIFFER +, DIFFERENT) 3D (OR DIMENSION?, SIZE?, SPACE+, SPACING, GAP+, WIDTH+, THICKNESS+),HEAT+,(CROSS+ 1W TALK+), CROSS-TALK+, CROSSTALK+

C. DOCUMENTS CONSIDERED TO BE RELEVANT

Category*	Citation of document, with indication, where appropriate, of the relevant passages	Relevant to claim No.
X	WO 2015021923 A1 (HUAWEI TECH CO LTD) 19 February 2015 (2015-02-19) description paragraphs 0023-0031, figures 3-12	1-8,12-16,19
Y	WO 2015021923 A1 (HUAWEI TECH CO LTD) 19 February 2015 (2015-02-19) description paragraphs 0023-0031, figures 3-12	9-11,17-18,20
Y	CN 103293714 A (UNIV JILI) 11 September 2013 (2013-09-11) description paragraphs 0011-0055, figures 1-3	9-11,17-18,20
A	US 6526203 B1 (ALCATEL OPTRONICS UK LTD) 25 February 2003 (2003-02-25) the whole document	1-20
A	US 5015066 A (EASTMAN KODAK CO) 14 May 1991 (1991-05-14) the whole document	1-20

☑ Further documents are listed in the continuation of Box C. ☑ See patent family annex.

* Special categories of cited documents:

"A" document defining the general state of the art which is not considered to be of particular relevance

"E" earlier application or patent but published on or after the international filing date

"L" document which may throw doubts on priority claim(s) or which is cited to establish the publication date of another citation or other special reason (as specified)

"O" document referring to an oral disclosure, use, exhibition or other means

"P" document published prior to the international filing date but later than the priority date claimed

"T" later document published after the international filing date or priority date and not in conflict with the application but cited to understand the principle or theory underlying the invention

"X" document of particular relevance; the claimed invention cannot be considered novel or cannot be considered to involve an inventive step when the document is taken alone

"Y" document of particular relevance; the claimed invention cannot be considered to involve an inventive step when the document is combined with one or more other such documents, such combination being obvious to a person skilled in the art

"&" document member of the same patent family

Date of the actual completion of the international search	Date of mailing of the international search report
19 July 2016	**28 July 2016**
Name and mailing address of the ISA/CN **STATE INTELLECTUAL PROPERTY OFFICE OF THE P.R.CHINA** **6, Xitucheng Rd., Jimen Bridge, Haidian District, Beijing 100088, China** Facsimile No. **(86-10)62019451**	Authorized officer **REN,Zhiwei** Telephone No. **(86-10)62085590**

INTERNATIONAL SEARCH REPORT

International application No.
PCT/CN2016/081533

C. DOCUMENTS CONSIDERED TO BE RELEVANT

Category*	Citation of document, with indication, where appropriate, of the relevant passages	Relevant to claim No.
A	CN 1362805 A (FURUKAWA ELECTRIC IND KK) 07 August 2002 (2002-08-07) the whole document	1-20
A	US 2002181868 A1 (MCGREER K) 05 December 2002 (2002-12-05) the whole document	1-20

INTERNATIONAL SEARCH REPORT
Information on patent family members

International application No.
PCT/CN2016/081533

Patent document cited in search report			Publication date (day/month/year)	Patent family member(s)			Publication date (day/month/year)
WO	2015021923	A1	19 February 2015	KR	20160034395	A	29 March 2016
				US	2015049998	A1	19 February 2015
				EP	3033642	A1	22 June 2016
				CN	105474057	A	06 April 2016
CN	103293714	A	11 September 2013	CN	103293714	B	28 October 2015
US	6526203	B1	25 February 2003	None			
US	5015066	A	14 May 1991	None			
CN	1362805	A	07 August 2002	US	6501882	B2	31 December 2002
				KR	20020055445	A	08 July 2002
				US	2002122627	A1	05 September 2002
				EP	1219989	A3	07 April 2004
				JP	2002202419	A	19 July 2002
				EP	1219989	A2	03 July 2002
US	2002181868	A1	05 December 2002	US	6853769	B2	08 February 2005
				US	2005129363	A1	16 June 2005
				AU	2002306422	A1	03 October 2002
				WO	02075409	A3	11 March 2004
				WO	02075409	A2	26 September 2002